Dysregulation of M segment gene expression contributes to influenza A virus host restriction

Brenda M. Calderon[1], Shamika Danzy[1], Gabrielle K. Delima[1], Nathan T. Jacobs[1], Ketaki Ganti[1], Megan R. Hockman[1], Graeme L. Conn[2], Anice C. Lowen[1], and John Steel[1]

Departments of Microbiology and Immunology[1] and Biochemistry[2], Emory University School of Medicine, Atlanta

Address correspondence to John Steel, john.steel@emory.edu

Abstract

The M segment of the 2009 pandemic influenza A virus (IAV) has been implicated in its emergence into human populations. To elucidate the genetic contributions of the M segment to host adaptation, and the underlying mechanisms, we examined a panel of isogenic viruses that carry avian- or human-derived M segments. Avian, but not human, M segments restricted viral growth and transmission in mammalian model systems, and the restricted growth correlated with increased expression of M2 relative to M1. M2 over-expression was associated with intracellular accumulation of autophagosomes, which was alleviated by interference of the viral proton channel activity by amantadine treatment. As M1 and M2 are expressed from the M mRNA through alternative splicing, we separated synonymous and non-synonymous changes that differentiate human and avian M segments and found that dysregulation of gene expression leading to M2 over-expression diminished replication, irrespective of amino acid composition of M1 or M2. Moreover, in spite of efficient replication, virus possessing a human M segment that expressed avian M2 protein at low level did not transmit efficiently. We conclude that (i) determinants of transmission reside in the IAV M2 protein, and that (ii) control of M segment gene expression is a critical aspect of IAV host adaptation needed to prevent M2-mediated dysregulation of vesicular homeostasis.

Author summary

Influenza A virus (IAV) pandemics arise when a virus adapted to a non-human host overcomes species barriers to successfully infect humans and sustain human-to-human transmission. To gauge the adaptive potential and therefore pandemic risk posed by a particular IAV, it is critical to understand the mechanisms underlying viral adaptation to human hosts. Here, we focused on the role of one of IAV's eight gene segments, the M segment, in host adaptation. Comparing the growth of IAVs with avian and human derived M segments in avian and mammalian systems revealed that the avian M segment restricts viral growth specifically in mammalian cells. We

39 show that the mechanism underlying this host range phenotype is a dysregulation of viral gene
40 expression when the avian IAV M segment is transcribed in mammalian cells. In particular,
41 excess production of the M2 protein results in viral interference with cellular functions on which
42 the virus relies. Our results therefore reveal that the use of cellular machinery to control viral
43 gene expression leaves the virus vulnerable to over- or under-production of critical viral gene
44 products in a new host species.
45

46 **Introduction**

47 Influenza A virus (IAV) epidemics and pandemics result in widespread and often severe disease
48 [1-3], as well as considerable societal economic costs [4]. IAV lineages endemic in humans are
49 ultimately derived from those circulating in wild waterfowl. Sporadic transmission of IAV from
50 avian reservoirs to humans occurs, mainly through domesticated intermediate hosts such as
51 chickens and pigs [5]. For example, infection of humans with H7N9 and H5N1 subtype IAVs
52 occurs through direct exposure to infected poultry. Although they often cause severe disease,
53 these zoonotic cases have not led to sustained onward transmission to date and have therefore
54 not caused a pandemic. Despite abundant circulation of IAVs at the animal-human interface,
55 pandemics occur only rarely owing to the host specificity of IAV infection. As with all viruses,
56 IAV must exploit host cell functions and overcome antiviral barriers to execute its life cycle. Viral
57 replication in a new host species therefore requires adaptation to re-establish virus-host
58 interactions broken by species-specific features of host cellular processes. IAV can undergo
59 such adaptation through reassortment of intact gene segments between avian IAVs and those
60 already adapted to mammals or through more incremental changes brought about by
61 polymerase error [6]. With the goal of anticipating and mitigating IAV emergence in humans, it is
62 essential to understand the species-specific barriers to infection and the mechanisms by which
63 IAV evolution allows these impediments to be overcome.

64 Changes to viral receptor specificity and polymerase function necessary to overcome host
65 species barriers have been well documented [7-11], but it is clear that additional features of
66 avian IAVs restrict their growth in mammalian systems [12-14]. A potential role for the M
67 segment was suggested by the *in silico* identification of positive selection acting on the M
68 segment of the Eurasian avian-like swine lineage, following transfer of this IAV from birds to
69 swine [15]. In addition, we and others have shown that the M segment of the 2009 pandemic
70 H1N1 (pH1N1) strain carries determinants of transmissibility, suggesting that adaptation of this
71 segment to humans contributed to the emergence of the pH1N1 lineage [16-20]. The

72 mechanistic basis for this contribution; the specific roles, if any, of M1 and M2 proteins to host
73 range; and whether the M segment plays a broader role in IAV host adaptation, remain unclear.
74 The M segment of IAV encodes the M1 matrix and the M2 proton channel proteins via
75 alternative splicing (**Suppl. Figure 1)** [21, 22]. M1 forms a structural layer under the viral
76 envelope and is a major determinant of virion morphology [16, 18, 23, 24]. Upon endocytosis of
77 virus particles into cells, low pH and high [K+] trigger a conformational change in M1 required
78 for release of viral ribonucleoprotein (vRNP) complexes into the cytoplasm [25]. M1 is also
79 critical for the transport of newly replicated vRNPs from the nucleus to the cytoplasm [26-29]. At
80 late stages of infection, cytoplasmic M1 is thought to recruit vRNP complexes to the budding
81 site [30-32].
82 M2 is a transmembrane protein that tetramerizes to form a proton channel. Within the envelope
83 of incoming virions, this channel allows diffusion of protons into the virion core, thereby
84 triggering the release of vRNPs from M1 [33-36]. M2 also plays an important role in the final
85 stages of virion morphogenesis, mediating ESCRT-independent membrane scission [37].
86 Importantly for the findings reported herein, multiple groups have reported that M2 blocks the
87 fusion of autophagosomes with lysosomes [38-40]. Under normal conditions, this fusion event
88 allows degradation and recycling of organelles and protein aggregates contained within
89 autophagosomes [41], and is thus important for cellular homeostasis. M2-mediated interference
90 with autolysosome formation therefore stalls autophagic flux and leads to the accumulation of
91 autophagosomes within the cell [38-40].
92 Many elegant molecular virological studies have revealed that viral strategies for regulating
93 gene expression are central to orchestration of the viral life cycle [42-45]. Here, we report that
94 regulation of M2 expression of IAV is an important determinant of host range. In particular, our
95 data show that the expression of M1 and M2 from alternatively spliced M segment mRNAs is
96 dysregulated when an avian IAV replicates in mammalian cells, and that the resultant over-
97 expression of the M2 proton channel attenuates viral growth by disrupting the cellular autophagy

98 pathway. The observed block in autophagy is consistent with that reported previously for lab-
99 adapted strains of IAV [38-40]. Importantly, however, we see that lab-adapted IAVs express M2
100 at high levels, comparable to those seen for avian IAV M segments in mammalian cells. In
101 contrast, IAVs carrying M segments well adapted to mammalian systems express relatively little
102 M2 and do not trigger the accumulation of autophagosomes to the same extent as avian-origin
103 and lab-adapted strains. These findings suggest that IAV-induced stalling of autophagic
104 turnover is a result of aberrantly high M2 expression upon infection of mammalian cells with
105 avian IAVs, and which is overcome in human-adapted influenza A lineages. Critically, the
106 mechanism leading to this host-restricted phenotype occurs at the level of gene expression and
107 is driven by host specific differences in nucleic acid sequence, not amino acid changes. This
108 mechanism constitutes a novel paradigm in RNA virus host adaptation, and reveals a novel
109 species barrier for IAV, which may be highly relevant for the emergence of avian IAVs into
110 humans.
111
112 **Results**
113 **Generation of isogenic IAVs differing only in the M segment**
114 To assess the contribution of the M segment to host adaptation, we generated a panel of IAVs
115 possessing human- or avian-adapted M segments in the A/Puerto Rico/8/34 (H1N1) [PR8]
116 background (**Table 1; Figure 1A; Suppl. Figure 1B, C, D**). The M segments used were
117 selected with the aims of representing circulating human IAVs and capturing the breadth of
118 diversity of M segment sequences present in wild waterfowl. In addition to three wild-type avian
119 M segments, we included in our panel a mutant of the dk/Alb/76 M segment that carries a
120 uniquely identified mutation in M2 (S89). Reversion of this unique amino acid residue to glycine
121 yields an M2 protein matching the consensus amino acid sequence of IAVs in wild bird
122 reservoirs. The human-adapted M segment analyzed most extensively herein is that of the
123 pandemic A/NL/602/09 (H1N1) strain [NL/09].

124

125 **Table 1. Origin of IAV M segments used in study**

Strain	Abbreviation	% Nucleotide identity to avian H1N1 subtype consensus	% M1 Amino acid identity to avian consensus (no. of a.a. differences)	% M2 Amino acid identity to avian consensus (no. of a.a. differences)
A/NL/602/2009 (H1N1)	NL/09	91.7	96.4 (9)	92.8 (7)
A/Panama/2007/99 (H3N2)	Pan/99	91.0	95.6 (11)	85.6 (14)
A/Bethesda/55/2015 (H3N2)	Beth/15	90.5	95.6 (11)	83.5 (16)
A/mallard/MN/19906/99 (H3N8)	Ma/MN/99	98.9	100	97.9 (2)
A/rhea/North Carolina/39482/93 (H7N1)	Rh/NC/93	98.7	100	100
A/duck/Alberta/35/76 (H1N1)	Dk/Alb/76	96.6	100	99 (1)
A/duck/Alberta/35/76 (H1N1) M2 89G	Dk/Alb/76 89G	96.7	100	100

126 a.a.: Amino acid residue.

127 **IAV M segments of avian origin confer a host-restricted phenotype**

128 The relative fitness of PR8-based viruses carrying M segments from the human-adapted NL/09
129 virus or from avian IAVs was evaluated in three avian substrates: embryonated chicken's eggs
130 (ECE), chicken origin DF-1 cells, and quail origin QT-6 cells. When grown from low multiplicities
131 of infection (MOI) in each of ECE and DF-1 cell substrates, all viruses exhibited similar kinetics
132 and reached comparable titers (**Figure 1B and 1C**). Also, under high MOI growth conditions in
133 DF-1 and QT-6 cells, the phenotypes of the PR8 NL/09 M and PR8 avian M viruses were similar
134 (**Figure 1D and 1E)**. At no time did the NL/09 M-encoding virus grow to significantly higher titers
135 than the avian M-encoding viruses in avian host substrates. In contrast, in mammalian cells,
136 human-adapted IAV M segments were found to support improved growth relative to avian-
137 adapted M segments. Viral growth was monitored from low and high MOI in human A549 cells
138 and canine MDCK cells (**Figure 2**), and additionally from high MOI in 293T cells (**Suppl. Figure**
139 **2A**). In each case, PR8-based viruses carrying the NL/09 M segment grew with more rapid
140 kinetics and to higher titers than isogenic viruses carrying avian M segments, although the
141 differences in growth from low MOI did not reach statistical significance. To extend our findings
142 to an independent human lineage of IAV, we evaluated the growth from high MOI in A549 cells
143 of PR8 Pan/99 M and PR8 Beth/15 M viruses, each of which have an M segment derived from

144 the human seasonal H3N2 lineage (**Suppl. Figure 1C, D**). We found that both of these human-
145 adapted M segments supported significantly faster kinetics and higher magnitude of growth than
146 the dkAlb76 (89G) M segment (**Suppl. Figure 2B**). Thus, results from multiple different avian
147 and mammalian culture systems reveal defects in the kinetics and magnitude of viral growth
148 associated with avian IAV M segments specifically in mammalian host cells, and provide
149 evidence of the acquisition of adaptive changes in the M segment of pH1N1 and H3N2 human
150 influenza A lineages.
151
152 **Avian IAV M segments confer lower viral infectivity, growth and transmission than NL/09**
153 **M segment in a guinea pig model**
154 To evaluate the impact of M segment host adaptation on viral phenotypes in an intact host, we
155 evaluated the PR8 NL/09 M virus and the four PR8-based viruses carrying avian M segments in
156 a guinea pig model [46, 47]. A low inoculation dose of 10 PFU per animal was used to maximize
157 the sensitivity of the system. Each inoculated animal was co-caged with a naïve guinea pig at
158 24 h post-inoculation and viral infectivity, magnitude and kinetics of growth, and transmission
159 were monitored by collecting nasal lavage samples every other day. Among those animals that
160 were productively infected, total virus sampled in nasal washes over the course of infection was
161 evaluated by calculating the area under the shedding curves shown in **Figure 3A**. Area under
162 the curve values did not differ significantly among the four viruses with avian M segments, but
163 were significantly higher for PR8 NL/09 M virus (**Figure 3A**). As shown in **Figure 3B**, fewer
164 guinea pigs were productively infected with 10 PFU when the inoculating virus carried an avian
165 M segment. Differences in the kinetics of viral growth were determined by assessing changes in
166 growth over time using repeated measures ANOVA (**Suppl. Figure 3**). Each virus encoding an
167 avian host derived M segment replicated with significantly slower kinetics than the PR8 NL09 M
168 virus.

169 The efficiency of transmission was assessed by calculating the proportion of contact animals
170 that contracted infection, considering only cages in which donor guinea pigs were productively
171 infected through intranasal inoculation. While transmission occurred in 7/9 instances for PR8
172 NL/09 M virus, a significantly lower proportion of animals (1/20; $p<0.0001$) were infected with a
173 virus carrying an avian M segment transmitted from her cage mate (**Figure 3B**). Thus, data from
174 a mammalian animal model reveal defects in infectivity, growth and transmission associated
175 with avian IAV M segments. Our results suggest the acquisition of adaptive changes in the M
176 segment of pH1N1 human IAV since its introduction from the avian reservoir into mammals.
177

178 **The M2 proton channel is aberrantly over-expressed from avian IAV M segments in**
179 **mammalian cells**

180 To investigate the mechanism underlying the host restricted phenotypes conferred by avian-
181 adapted M segments, the steady state levels of the M1 and M2 proteins were evaluated in
182 human A549 and avian DF-1 cells infected at high MOI. Western blotting with the monoclonal
183 antibody E10, which recognizes the shared N-terminus of M1 and M2, was used to monitor
184 levels of both proteins concurrently.
185 In the avian cell line, the PR8 NL/09 M virus expressed lower levels of M2 than M1 (**Figure 4A**).
186 When M1 and M2 levels were normalized to those of vinculin and the relative levels of M1 and
187 M2 calculated, the NL/09 M2 protein comprised <10% of the total M segment derived protein
188 expression. Very similar results were seen for four PR8-based viruses carrying avian M
189 segments grown in DF-1 cells. In each case, M2 comprised <20% of the total M segment
190 derived protein, and in the case of three avian M segment-containing viruses (PR8 dkAlb76 M;
191 PR8 dkAlb76 M 89G; and PR8 rheaNC M), the levels of M1 and M2 proteins were not
192 significantly different from those expressed by the PR8 NL/09 M virus (**Figure 4B, 4C, 4D**).
193 In A549 cells, the PR8 NL/09 M virus expressed M2 at ~20% of the total M protein, similar to the
194 expression levels observed in infected DF-1 cells (**Figure 5A**). In contrast, avian M segments

195 yielded markedly higher levels of the M2 protein than were observed for the same viruses grown
196 in avian cells. Here, M2 levels were approximately equal to those of M1 (**Figure 5B, 5C, 5D**).
197 Moreover, when compared to the NL/09 M segment in human cells, levels of M2 protein were
198 significantly higher for avian M segments ($P<0.0001$) (**Figure 5C, 5D**). Thus, compared to
199 matched virus-host pairings in both human and avian systems, M2 was markedly over-
200 expressed when avian-adapted M segments were introduced into human cells.
201
202 **Over-expression of M2 protein in mammalian cells corresponds to increased levels of the**
203 **M2 mRNA (mRNA 10)**
204 The M segment vRNA is transcribed by the viral polymerase to give rise to a co-linear mRNA
205 ($mRNA_7$), which can be spliced by cellular splicing factors to yield $mRNA_{10}$ or $mRNA_{11}$ [48, 49].
206 The M1 protein is translated from the unspliced $mRNA_7$, while M2 is expressed from the spliced
207 $mRNA_{10}$. To date, no polypeptide corresponding to the short $mRNA_{11}$ ORF has been identified.
208 Aberrantly high levels of IAV $mRNA_{10}$ in mammalian cells have been previously reported for the
209 avian IAV, fowl plague virus [50, 51]. We therefore hypothesized that the high expression levels
210 of M2 protein, observed for avian adapted M segments in human cells, was due to increased
211 splicing of $mRNA_7$ to yield excessive $mRNA_{10}$. We used a primer extension assay to quantify the
212 levels of each M segment-derived mRNA species in DF-1 and A549 cells infected with either
213 PR8 NL/09 M virus or one of four viruses carrying an avian-adapted M segment.
214 As expected, based on the levels of the encoded proteins, $mRNA_{10}$ was of low abundance
215 compared to $mRNA_7$ for all viruses in DF-1 cells (**Figure 6A**). Quantification of band intensities
216 revealed that, in DF-1 cells infected with PR8 NL/09 M virus, $mRNA_7$ comprised ~75%, while
217 $mRNA_{10}$ comprised ~5% of the total M segment derived mRNA (**Figure 6B**). For three avian M
218 viruses (PR8 dkAlb76 M; PR8 dkAlb76 M 89G; and PR8 rheaNC93 M), relative levels of $mRNA_7$
219 were ~70-75% and were not significantly different from those of PR8 NL/09 M virus (**Figure 6B**).
220 For all viruses, $mRNA_{10}$ was expressed at low levels (10-40% of total segment 7 mRNA), and in

221 the case of two avian M segment-containing viruses (PR8 dkAlb76 M; PR8 dkAlb76 M 89G), the
222 levels of $mRNA_{10}$ were not significantly different from those expressed by the PR8 NL/09 M
223 virus (**Figure 6C**). $mRNA_{11}$ was expressed in each infection at approximately 20% of the total M
224 segment derived mRNA, and the relative level did not differ significantly with any virus (**Figure**
225 **6D**). Overall, the relative levels of each of the three mRNA species were similar when
226 synthesized from avian- or human-origin encoded M segments in DF-1 cells, correlating with
227 western blot data on M segment protein expression in these cells.
228 In A549 cells, the PR8 NL/09 M virus showed relatively high abundance of $mRNA_7$ and low
229 abundance of $mRNA_{10}$, as was seen in DF-1 cells (**Figure 7A**). By contrast, for viruses carrying
230 avian adapted M segments, $mRNA_{10}$ levels exceeded those of $mRNA_7$ in this human cell line
231 (**Figure 7B, 7C**). Again, no significant differences in relative $mRNA_{11}$ levels among the viruses
232 were noted (**Figure 7D**) suggesting that changes in splicing to produce $mRNA_{11}$ do not
233 contribute to changes in M segment mRNA and protein expression observed in A549 cells.
234 Overall, our data point to increased splicing to produce $mRNA_{10}$ as the underlying mechanism
235 leading to heightened M2 expression from avian M segments in A549 cells, and suggest that
236 cis-acting signals present on the M segment are responsible for driving the disparate M2
237 expression levels.
238
239 **M2 expressed from avian M segments localizes in perinuclear puncta**
240 To gain initial insight into the phenotypic consequences of M2 overexpression, we examined the
241 subcellular localization of M2 in A549 cells infected with PR8 NL/09 M virus or one of four PR8-
242 based viruses with avian M segments. At 8 hours-post-infection (hpi) in PR8 NL/09 M virus-
243 infected cells, M2 showed mainly dispersed cytoplasmic staining, along with weak cytoplasmic
244 membrane localization and some perinuclear accumulation. By contrast, in cells infected with
245 viruses that encoded any of the four avian origin M segments, we noted more abundant M2
246 protein staining localized at the plasma membrane, and in large puncta near the cell nucleus

247 (**Figure 8A, 8B**). Similar data were obtained from virus-infected 293T cells at 8 hpi (**Figure 8C,**
248 **8D**) and from both human cell lines at 12 hpi (**Suppl. Figure 6**). This staining pattern, along with
249 data in previously published studies [38-40], prompted us to investigate whether highly
250 expressed M2 protein was interacting with the cellular autophagy pathway.
251

252 **Human cells exhibit increased LC3B II levels when infected with IAV carrying avian M**
253 **segments**

254 An interaction between the IAV M2 protein and the cellular autophagy pathway has been
255 reported previously [38-40]. To test whether M2 expression from avian vs. human M segments
256 has differential effects on autophagy, we first evaluated the level of LC3B lipidation in PR8
257 NL/09 M- and PR8 avian M-infected cells. Upon activation of the autophagy pathway, LC3B is
258 modified through the addition of phosphotidylethanolamine [52, 53]. This lipidated form is called
259 LC3B II and it remains associated with the membranes of maturing and mature
260 autophagosomes. Thus, increased levels of LC3B II in the cell are indicative of autophagosome
261 formation; however, under normal conditions LC3B I and II are cycled through an autophagic
262 flux which involves autophagosome maturation and degradation via fusion with lysosomes [54].
263 A block in this fusion event can therefore lead to accumulation of autophagosomes in the
264 cytoplasm and, consequently, accumulation of LC3B II in the cell.

265 Western blot analysis of LC3B revealed decreased LC3B I, and increased LC3B II protein levels
266 in virus-infected cells compared to mock, providing evidence of autophagy activation and/or
267 block during IAV infection of either avian or human cells (**Figure 4A, 4E, 4F; 5A, 5E, 5F**). In
268 avian DF-1 cells, levels of LC3B I were slightly decreased and levels of LC3B II were slightly
269 increased over mock, but LC3B I and LC3B II levels were generally comparable among human
270 M- and avian M-containing viruses (**Figure 4E, 4F**). Importantly, human A549 cells infected
271 with PR8 avian M-containing viruses consistently showed lower levels of LC3B I, and higher
272 levels of LC3B II than A549 cells infected with PR8 NL/09 M as well as other human M-

273 containing viruses (**Figure 5E, 5F).** Additionally, the same phenotypes were obtained from the
274 panel of viruses upon infection of human origin 293T cells (**Suppl. Figure 4A-4F**), or canine
275 origin MDCK cells (**Suppl. Figure 4G-4L**).
276 Taken together, these data reveal a correlation between levels of M2 expression and LC3B
277 lipidation (accumulation of LC3B II), suggesting that high levels of M2 present in PR8 avian M-
278 infected cells may be inducing an over-activation of autophagy, or a block in the turnover of
279 autophagosomes.
280
281 **Infection of human cells with IAV carrying avian M segments triggers accumulation of**
282 **autophagosomes**
283 To confirm that M2 protein was co-localizing with LC3-positive autophagic vesicles in
284 mammalian cells, we monitored sub-cellular localization of an overexpressed LC3B-GFP fusion
285 protein in infected cells. Human 293T cells were primarily used for this purpose as they
286 transduce well with GFP-LC3. Under normal conditions, LC3B-GFP can be seen throughout the
287 cell with a diffuse distribution (**Figure 9, row 1: mock infected cells**). Treatment with
288 chloroquine, an inhibitor of autophagy that decreases autophagosome-lysosome fusion, results
289 in the concentration of LC3B-GFP into punctate cytoplasmic structures (**Figure 9, row 7: CQ-**
290 **treated cells**). This relocalization is indicative of the accumulation of autophagosomes [55]. In
291 LC3B-GFP expressing 293T cells infected with PR8 NL/09 M virus, we observed a slight
292 increase in GFP-positive cytoplasmic puncta (**Figure 9, row 2: NL09 M infected cells**). In cells
293 infected with PR8 avian M-encoding viruses, by contrast, extensive accumulation was apparent,
294 with both the size and number of intracellular vesicles increased relative to PR8 NL/09 M
295 infection (**Figure 9, rows 3-6: Avian M infected cells**). In addition to these cytoplasmic puncta,
296 viruses with avian M segments were found to redirect a small proportion of LC3B-GFP to the
297 plasma membrane. Notably, the M2 protein co-localized with LC3B-GFP in PR8 avian M
298 infected cells, both in cytoplasmic puncta and at the plasma membrane. Similar phenotypes

299 were observed in virus-infected A549 cells, at 8 hpi **(Suppl. Figure 7**). Overall, these results
300 suggest that expression of avian M2 protein at high levels interferes with the turnover of
301 autophagosomes and with the localization of LC3B-GFP. In addition, the results reveal a
302 reduction in the tight perinuclear localization of M2 upon LC3B overexpression.
303 As an additional test designed to differentiate autophagy induction from autophagy block in cells
304 infected with IAV carrying avian M segments, we used chloroquine treatment followed by
305 western blotting for LC3B I and LC3B II. We hypothesized that, if autophagic flux is blocked in
306 cells infected with PR8 avian M viruses, then treatment with chloroquine would not lead to a
307 further increase in LC3B II levels. Conversely, if virus infection of these cells induces autophagy,
308 then blocking their turnover with chloroquine would result in heightened LC3B II over mock
309 infected, chloroquine-treated cells. As shown in **Suppl. Figure 8A and 8C**, we observed a
310 significant difference in the activation of LC3B II following infection with human or avian M-
311 encoding viruses. This difference in LC3B II activation is lost in the presence of chloroquine.
312 Additionally, as we observed no change in LC3B II levels upon treatment of virus-infected cells
313 with chloroquine, relative to chloroquine-treated, mock infected cells, we conclude that the high
314 levels of IAV M2 protein expressed from avian M segments, but not human M segments,
315 precipitate a block in the autophagy pathway such that chloroquine treatment cannot bring
316 about further accumulation of autophagosomes.
317

318 **Ion channel activity of IAV M2 contributes to LC3B II accumulation in A549 cells**

319 To evaluate the contribution of IAV M2 ion channel activity to the observed stalling of autophagy
320 in PR8 avian M virus-infected cells, we inhibited channel activity with amantadine [56].
321 Amantadine was added at 1 hpi and the level of LC3B lipidation was assessed at 8 hpi in PR8
322 NL/09 M and PR8 avian M virus-infected A549 cells. The timing of amantadine addition was
323 designed to avoid disruption of the early function of M2 in delivery of the viral genome to the
324 cytoplasm, but allow inhibition of M2 activity in autophagosomes.

325 As noted above (**Figure 5; Suppl. Figure 4**), western blot analysis of LC3B revealed decreased
326 LC3B I and increased LC3B II upon infection of A549, 293T or MDCK cells, with avian or human
327 M-encoding IAV, with the effect being stronger for viruses possessing avian M segments.
328 Interestingly, addition of amantadine reversed the intracellular accumulation of LC3B II in both
329 human and Av M infected A549 cells (**Figure 10**). Quantitation of M segment-encoded proteins
330 by western blot showed no difference in the expression levels of M1 or M2 protein upon
331 treatment with amantadine (**Figure 10 A, 10B, 10C, 10D**), but revealed a statistically significant
332 increase in LC3B I (**Figure 10E**) and decrease in LC3B II (**Figure 10F**) to levels comparable to
333 mock infected cells.
334 To ensure that the amantadine was working to prevent LC3B II accumulation through inhibition
335 of M2 ion channel activity, we assessed the impact of amantadine treatment on the inhibition of
336 phagosome-lysosome fusion by chloroquine. Amantadine had no impact on LC3B II
337 accumulation in the absence of M2 protein (**Figure 10G-I**), indicating that the mechanism of
338 amantadine block of autophagosome accumulation was specifically mediated through
339 interference with M2 function.
340 As a complementary approach to monitor the effects of amantadine, we again used
341 overexpressed LC3B-GFP fusion protein in infected 293T cells at 12 hpi. Using confocal
342 microscopy, we tracked LC3B-GFP localization in the presence and absence of the ion channel
343 blocker. In line with the western blot analyses obtained in A549 cells, we saw that amantadine
344 reduced the accumulation of LC3B-GFP within cytoplasmic puncta and at the plasma
345 membrane of infected cells (**Figure 11**). Of note, amantadine treatment did not alter levels or
346 localization of M2 protein and, moreover, had no detectable effect on LC3B-GFP appearance in
347 chloroquine-treated cells (**Figure 11**).
348 Overall, our results indicate that the intracellular ion channel activity of IAV M2 protein is
349 necessary to mediate the observed block in autophagy, and that addition of amantadine can
350 reverse the autophagic phenotypes induced by both human and avian M-encoding IAVs.

351

352 **Improved viral growth in the presence of amantadine implicates autophagy block in viral**
353 **growth restriction**

354 To test for a causal link between the observed block in autophagy and the restriction of growth
355 seen for PR8 avian M-encoding viruses in mammalian cells, we monitored the effect on viral
356 growth of relieving the autophagy block with amantadine treatment. Specifically, we evaluated
357 single cycle growth in A549 cells using PR8 NL/09 M and PR8 dkAlb76 M 89G viruses.
358 Amantadine was again added at 1 hpi to avoid disruption of the earliest steps of the viral life
359 cycle. While amantadine had no effect on growth of the PR8 NL/09 M virus (P=0.271), a modest
360 but consistent increase in the titer of PR8 dkAlb76 M 89G virus was noted throughout the time
361 course (P=0.0007) (**Figure 12**). This result indicates that M2 ion channel-induced disruption of
362 vesicular homeostasis contributes to the host restriction conferred by avian IAV M segments.

363

364 **Viral growth restriction and autophagy block are linked to M2 expression levels, not**
365 **amino acid sequence**

366 To determine whether the observed effects of avian-origin M segments on the viral life cycle and
367 the autophagy pathway are attributable to avian-adapted amino acid sequences or rather to the
368 over-expression of the viral proton channel, we generated a series of chimeric M segments in
369 which the coding changes found in the NL/09 M segment were transferred to an avian adapted
370 RNA background, and vice versa. We introduced all 16 coding changes into M1 and M2
371 simultaneously, or introduced only the nine or seven changes into M1 or M2, respectively. The
372 genotypes of this panel of six chimeric viruses are outlined in **Table 2** and **Suppl. Figure 9**.

373

374 **Table 2. Genotypes of avian-human chimeric M segments**

	Nucleic acid background	M1 amino acid sequence	M2 amino acid sequence
NL M 16mut	NL/09 M	Avian consensus M1	Avian consensus M2
NL M 9mut	NL/09 M	Avian consensus M1	NL/09 M2

NL M 7mut	NL/09 M	NL/09 M1	Avian consensus M2
Av M 16mut	Dk Alb 76 M 89G	NL/09 M1	NL/09 M2
Av M 9mut	Dk Alb 76 M 89G	NL/09 M1	Avian consensus M2
Av M 7mut	Dk Alb 76 M 89G	Avian consensus M1	NL/09 M2

375

376 Western blot analysis of M1 and M2 proteins expressed from these six chimeric M segments in
377 infected A549 cells is shown in **Figure 13A**. Among the viruses with the NL/09 M nucleic acid
378 background, the PR8 NL M 16mut and PR8 NL M 9mut viruses both showed increased levels of
379 M2 relative to the PR8 NL/09 M virus control, indicating that all or some of the coding changes
380 introduced into the M1 ORF impact regulation of M2 gene expression. The PR8 NL M 7mut
381 virus showed similar M1 and M2 expression levels as the PR8 NL/09 M control, however. This
382 virus therefore expresses the avian consensus M2 protein at low levels. All viruses with the
383 nucleic acid background of the avian M segment showed relatively high levels of M2, similar to
384 those seen for the PR8 dkAlb76 M 89G virus control. Thus, in the avian nucleic acid
385 background, we were able to fully separate M2 expression level from M2 and M1 amino acid
386 sequence.
387 Single cycle growth analysis of the chimeric viruses in A549 cells revealed a strong correlation
388 between M2 expression level and viral yields (**Figure 14A, B and C**). Notably, all viruses with
389 the dkAlb76 M 89G derived nucleic acid background, which express high levels of M2 protein,
390 grew to approximately 10-fold lower titers than the PR8 NL/09 M virus, despite expression of
391 NL/09 M1 and/or M2 proteins. In addition, the PR8 NL M 7mut virus, which expresses the
392 human M1 and avian M2 proteins at levels typical of human-adapted strains, showed equivalent
393 growth to that seen with the PR8 NL/09 M virus, indicating that amino acid changes in M2 are
394 not required for efficient replication in human cells. Notably, the PR8 Av M 9mut virus, which
395 encodes identical M1 and M2 proteins as PR8 NL M 7mut virus (**Suppl. Figure 9**), exhibits
396 approximately 10-fold reduced viral replication relative to PR8 NL M 7mut virus (P=0.0003)
397 (**Figure 14B and C**). This result confirms that over-expression of M2 protein is a dominant
398 negative trait that is deleterious to virus growth.

399 Examination of LC3B lipidation by western blot analysis also revealed a clear correlation
400 between M2 expression levels and those of LC3B II within infected cells (**Figure 13A**).
401 Importantly, overexpression of either human or avian M2 during infection boosted LC3B II levels
402 (compare lanes 2, 3, 5, 6, 7 and 8 in **Figure 13A**), while expression of Av M2 at levels
403 comparable to those of PR8 NL/09 M virus gave low LC3B II levels (compare lanes 1 and 4 in
404 **Figure 13A**). Confocal images of 293T cells transduced with LC3B-GFP and infected with the
405 chimeric viruses were consistent with these findings. As seen for wild type avian M segments,
406 high M2 expression again led to the accumulation of LC3B-GFP in perinuclear puncta and at the
407 plasma membrane (**Suppl. Figure 10**). Thus, as with viral growth, the accumulation of
408 autophagosomes within infected cells appears to be triggered by high levels of M2, regardless
409 of amino acid sequence.
410 To verify that the levels of M1 and M2 protein exhibited by the chimeric M segment-encoding
411 viruses are modulated at the level of mRNA expression, we conducted RT primer extension
412 assays. These data confirmed that differences in the levels of segment 7 mRNA expression
413 (**Suppl. Figure 11**) mirrored the observed differences in M1 and M2 protein expression levels.
414 Overall, these data support the premise that splicing signals are at least partly encoded in non-
415 synonymous nucleotide changes residing in the M1 ORF.
416
417 **Chimeric M segment expressing NL/09-like levels of NL/09 M1 and avian M2 supports**
418 **robust growth in vivo**
419 To evaluate whether correcting expression of the Av M2 protein to levels seen for viruses with
420 human-adapted M segments yielded a well-adapted phenotype in a mammalian animal model,
421 we evaluated growth and transmission of PR8 NL/09 M 7mut virus in guinea pigs. Titration of
422 nasal wash samples revealed that the PR8 NL/09 M 7mut virus (which expresses Av M2 at low
423 levels) had a similar growth phenotype to that of PR8 NL/09 M virus: growth kinetics and area
424 under the curve values were not significantly different (**Figure 15; Suppl. Figure 12**). In

425 contrast, analysis of nasal wash samples collected from contact animals indicated that only one
426 of eight inoculated guinea pigs transmitted the PR8 NL/09 M 7mut virus to her cage mate. This
427 level of transmission is significantly decreased relative to the PR8 NL/09 M virus (p=0.0339)
428 (**Figure 3B**). Taken together, these results indicate that, when expressed at levels typical for a
429 human-adapted M2 protein, an avian M2 supports efficient replication but inhibits transmission
430 in a mammalian host.
431
432 **Lab-adapted IAV, but not recent human isolates, express abundant M2 and block**
433 **autophagy in human cells**
434 The M2-induced block in autophagic flux reported previously was based on multiple IAVs that
435 were originally isolated from human hosts but passaged extensively in laboratory substrates
436 [38-40]. To assess whether these prior data were consistent with our own, we compared M2
437 expression levels exhibited by one of the lab-adapted strains used, PR8. Our results show that
438 the relative expression levels of M1 and M2 in PR8 infected 293T cells are comparable to those
439 seen in cells infected with avian M-encoding viruses (**Suppl. Figure 13**). These results suggest
440 that prior reports of M2-induced block in autophagy reflect a feature of mal-adaptation to the
441 host cell.
442
443 **Discussion**
444 Our data indicate that dysregulation of gene expression from the IAV M segment contributes to
445 the limited replicative capacity of avian IAVs in mammalian hosts. When transcribed within
446 mammalian cells, avian IAV M segments gave rise to abundant $mRNA_{10}$ and correspondingly
447 high levels of the encoded M2 proton channel. Comparison to matched virus-host systems
448 indicated that this M2 expression profile was an aberrant feature of avian IAV replication in
449 mammalian cells. When present at high levels, M2 had marked effects on the infected cell,
450 blocking the turnover of autophagic vesicles and redirecting LC3B II, the activated form of a

451 critical autophagy mediator, to the plasma membrane. These effects were found to rely on the
452 proton channel activity of M2 and occurred when either the avian or human M2 protein was
453 overexpressed in infected cells. Importantly, the reduction in viral growth conferred by avian M
454 segments in mammalian systems could be attributed at least in part to disruption of vesicular
455 homeostasis and was fully attributed to M2 overexpression. Thus, our data identify the
456 regulation of viral gene expression as a novel host-dependent feature of the IAV lifecycle that
457 contributes to the host range restriction of this virus.
458 Quantification of IAV encoded mRNAs within infected cells indicated that overexpression of M2
459 from avian IAV M segments stems from over-production of the corresponding mRNA. M2 is
460 encoded by the $mRNA_{10}$ transcript, which is generated through splicing of the M1 message,
461 $mRNA_7$ [48, 49]. Thus, regulation of M2 gene expression is intimately linked to the cellular
462 splicing machinery. Our data indicate that this is a finely balanced interaction between IAV and
463 its host cell, which is susceptible to disruption upon transfer to new species. In this regard, it is
464 notable that the M segment splice donor and acceptor sites are identical between the human
465 and avian IAVs examined. M segment sequences outside of these canonical splice sites have,
466 however, been shown to modulate splicing efficiency [57-60]. Interestingly, $mRNA_7$ association
467 with mammalian SF2/ASF [59], and with mammalian hnRNPK and NS1-binding protein [60],
468 have been shown to alter the efficiency of splicing. Nucleotide differences in these binding
469 regions exist between human- and avian-adapted M segments. An interesting area of further
470 investigation will be to test whether there are differences in the binding of human and avian
471 $mRNA_7$ molecules to mammalian SF2/ASF, hnRNPK and NS1-binding proteins.
472 The gene segments of IAVs circulating in humans are ultimately derived from the avian IAV
473 gene pool. Thus, the contrasting phenotypes conferred by avian- and human-adapted M
474 segments in mammalian cells suggest that a resetting of M segment gene expression to reduce
475 M2 levels has been positively selected following emergence of avian IAVs into mammalian
476 populations. Indeed, our data reveal that this adaptation has occurred in at least two

477 independent incidences: i) within the Eurasian avian-like swine lineage M, that emerged from
478 birds in the late 1970s and contributed the M segment to the pH1N1 virus prior to 2009; and ii)
479 within the human seasonal lineage derived from the 1918 pandemic, which contributed its M
480 segment to the H3N2 lineage represented by Pan/99 virus. The timing of the adaptive changes
481 is unclear in each case, and cannot be inferred from our data. Importantly, M2 expression in
482 human IAV mimics that of avian IAV in avian cells. Thus, restriction of splicing efficiency to
483 achieve low M2 levels appears to be an important feature of IAV host adaptation. Our data
484 furthermore suggest that the negative impact of an autophagy block on viral growth constitutes
485 an important pressure driving this selection.
486 To date, most publications related to autophagy in IAV infected cells have used the PR8 or
487 WSN lab-adapted strains, the X31 variant of PR8, or avian IAVs [38, 39, 61, 62]. We found that
488 PR8 virus expresses levels of M2 in mammalian cells that are comparable with avian IAVs. This
489 phenotype may be a result of adaptation to growth in chicken eggs. Owing to the use of viruses
490 carrying lab-adapted M segments, the current literature suggests that IAV infection routinely
491 induces a block in autophagy [38, 39, 61, 62]. We also see evidence of such a block when using
492 viruses that express high levels of M2, but we propose that this phenotype is a symptom of poor
493 adaptation to the mammalian host cell. Analysis of viruses carrying human M segments in
494 mammalian cells suggests that low levels of M2 and activation, but not blocking, of autophagy
495 are the norm in IAV infected cells.
496 While the previously reported block in autophagy induced by IAV has generally been interpreted
497 as a viral defense against an antiviral mechanism, a pro-viral role for autophagy is not without
498 precedent. In Dengue virus infection, autophagy has been reported to support viral replication.
499 Specifically, autophagic turnover of lipid droplets in infected cells is thought to provide energy
500 needed for viral growth and to supply phospholipids important during virion assembly [63-65].
501 For IAV, the availability of activated LC3B protein was reported to be important for viral
502 morphogenesis [38]. Specifically, M2 was implicated in recruitment of LC3B II to the plasma

503 membrane, and disruption of this recruitment was found to affect budding and reduce stability of
504 released virions [38]. We also noted strong redistribution of LC3B-GFP to the plasma
505 membrane during infection with viruses that express high levels of M2. This relocalization
506 occurred to a lesser extent in a well-matched IAV-host system (NL/09 M in human cells), and
507 may play a functionally important role in this context. A role for LC3B II in morphogenesis is
508 consistent with the activation of autophagy having a proviral effect. Conversely, our data
509 indicate that a block in autophagic turnover reduces viral growth, potentially owing to disruption
510 of vesicular trafficking that is normally exploited by the virus [66-68], or due to disruption of
511 cellular metabolic functions on which the virus relies.
512 By inhibiting the proton channel activity of the avian M2 with amantadine, we found that a
513 functional channel is needed to bring about the observed effects on autophagy. Indeed, M2 has
514 been shown previously to block the fusion of autophagosomes with lysosomes in a proton
515 channel-dependent fashion [61]. Surprisingly, however, amantadine treatment was also found to
516 reduce LC3B II accumulation in PR8 NL/09 M infected cells. The pH1N1 M2 protein carries the
517 S31N mutation, which confers resistance to amantadine. Our data suggest that this resistance
518 is not effective at a relatively high concentration of 200 μM amantadine, at least in the context of
519 intracellular viral infection.
520 The mutagenesis of the M segment that we carried out with the goal of separating the effects of
521 M2 expression level from M2 amino acid sequence revealed an important constraint on M1
522 coding capacity. Namely, the human / avian amino acid polymorphisms introduced into the M1
523 ORF were found to impact regulation of M2 gene expression. Some or all of these non-
524 synonymous changes to M1 likely modulate the efficiency of $mRNA_7$ splicing. With this new
525 insight in mind, a fresh look at viral phenotypes previously attributed to M1 amino acid variations
526 is warranted. Effects of M1 amino acid sequence on virion morphology [17, 23, 24, 69, 70], for
527 example, may in fact be directly or indirectly mediated through changes in intracellular M2
528 expression level.

529 Notably, while an avian M2 protein was sufficient to support robust viral replication in
530 mammalian systems when expressed at low levels, this sufficiency did not extend to
531 transmission. Virus expressing the avian M2 from a human M segment transmitted poorly,
532 indicating that the IAV M2 carries viral determinants of transmission and that these determinants
533 are not well conserved between avian and human strains. This novel observation also supports
534 the notion that high replicative capacity of a virus in a given host species is not necessarily
535 sufficient for transmission between individuals. In this context, it will be interesting to evaluate
536 the impact of avian M2 amino acid signatures on virion stability in the environment.
537 In summary, our data suggest that adaptive change in the M segment is needed to maintain low
538 expression of M2 in mammalian cells and that, in the absence of such adaptive changes,
539 excess M2 limits viral growth by blocking the autophagy pathway. These findings establish
540 regulation of viral gene expression as a feature of the virus-host interface critical for IAV host
541 range determination and therefore emergence into novel host populations.
542
543 **Materials and Methods**
544
545 *Cells*
546 Madin-Darby Canine Kidney (MDCK) cells (a kind gift of Peter Palese, Icahn School of Medicine
547 at Mount Sinai) were maintained in minimal essential medium (Gibco) supplemented with 10%
548 fetal bovine serum (FBS) and penicillin-streptomycin. A549 and 293T cells were obtained from
549 the ATCC and maintained in Dulbecco's minimal essential medium (DMEM; Gibco)
550 supplemented with 10% FBS and penicillin-streptomycin. DF-1 cells were obtained from ATCC
551 and maintained in DMEM plus 5% FBS and penicillin-streptomycin. QT-6 cells were obtained
552 from ATCC and maintained in F-12K medium plus 5% FBS, 10% tryptose phosphate and
553 penicillin-streptomycin. All cells were incubated at 37°C with 5% CO_2.
554

555 *Viruses*

556 All viruses used in this work were generated using reverse genetics techniques [71]. The
557 rescue system for PR8 was a gift of Peter Palese (Icahn School of Medicine at Mount Sinai).
558 The rescue system for A/Panama/2007/99 (H3N2) [Pan/99] virus was initially described in [7];
559 and that for A/Netherlands/602/2009 (H1N1) [NL/09] virus was a gift of Ron Fouchier (Erasmus
560 Medical Center) [72]. The NL/09 virus was propagated in MDCK cells for two passages. All
561 other virus stocks were generated in 10-11 day old embryonated chicken's eggs.

562

563 *Generation of chimeric M segments*

564 Non-synonymous nucleotide changes differentiating NL/09 and avian consensus M segments
565 were introduced in a reciprocal fashion into i) M1 and M2 to generate 16 mut viruses, ii) M1-only
566 to generate 9 mut viruses, and iii) M2-only to generate 7 mut viruses. The modified viral cDNAs
567 were synthesized by Genewiz and subcloned into the pDZ reverse genetic vector [73].

568

569 *Sequence alignments and generation of consensus sequences*

570 Alignment of the FASTA sequences downloaded from Genbank (or GISAID) databases was
571 carried out using DNASTAR Lasergene 13 MegAlign software running the Clustal W
572 phylogenetic alignment algorithm.

573 To obtain a consensus nucleotide sequence and to assess the degree of variability in the M
574 segment of H1N1 subtype avian IAVs, we searched the Genbank nucleotide database for full
575 length M segment sequences derived from avian H1N1 subtype IAV collected between 1976
576 and 2008 from any temperate Northern hemisphere location. We obtained 262 sequences,
577 which included sequences with partial 3' and 5' UTRs, and manually curated the sequences to
578 (i) remove swine and human lineage derived H1N1 M segments, retaining 247 sequences, and
579 (ii) trim UTR sequences from the retained segments. Alignment of the sequences by Clustal W

580 provided a working consensus sequence and revealed up to 7% variability at the nucleotide
581 level among the selected avian host-derived sequences.
582 To assess the degree of amino acid variability in the M segment of avian IAV of any subtype we
583 searched Genbank for full length M1 or M2 protein sequences derived from avian H1Nx to
584 H16Nx subtype IAV, collected between 1970 and 2000, from any geographical location. These
585 dates were chosen to avoid selecting sequences representing isolates originating from the
586 repeated H5 subtype HPAI incursions into poultry populations which dominate the Genbank
587 database from the early 2000s onwards, and which would likely bias the subsequent analysis.
588 For each hemagglutinin subtype (H1Nx to H16Nx), we aligned the available sequences to
589 generate individual consensus M1 and M2 amino acid sequences (**Supplemental Table 1**), and
590 aligned those consensus sequences to the avian H1N1 subtype consensus M1 and M2
591 sequences, in order to assess amino acid diversity. The matrix proteins of each subtype, with
592 the exception of H9Nx, were 100% conserved. The H9Nx subtype matrix protein shared 97.6%
593 identity to the avian H1N1 sequence. The M2 proteins of each subtype were 100% conserved,
594 excepting H9Nx, H13Nx and H16Nx subtypes, which shared 97.2%, 94.8% and 93.8% identity
595 respectively, to the avian H1N1 consensus sequence. Thus, the amino acid composition of M1
596 and M2 proteins are highly conserved within wild waterfowl, particularly within isolates that
597 circulate among dabbling ducks and geese. In these host species, both M1 and M2 proteins are
598 at, or close to, 100% identity at the consensus amino acid level.
599 To identify a consensus nucleotide sequence for the 2009 pH1N1 IAV, and compare it to the
600 avian consensus sequence, we searched Genbank for full-length M segments derived from
601 pH1N1 subtype IAV isolated in North America, collected between the 7th June and the 20th June
602 2009, which was shortly after emergence of the pH1N1 lineage into the human population. 189
603 individual nucleotide sequences were obtained, curated, and aligned, to provide a working
604 consensus sequence for the pH1N1 M segment. The pH1N1 M segments possessed >2%
605 variability at the nucleotide level. The A/NL/602/09 (H1N1) (NL09) M segment is a 100% match

606 to the consensus sequence of the 2009 pH1N1 lineage at the nucleotide level, and the M
607 segment from this strain was adopted for use throughout the current study. Interestingly,
608 comparison of the NL09 M segment to the avian consensus sequence revealed 8.3% difference
609 at the nucleotide level, and 9 and 7 amino acid changes in M1 and M2 proteins, respectively
610 (**Table 2**). These data suggest that pH1N1 M segment possesses a nucleotide sequence that is
611 highly divergent from M segments obtained from viruses circulating within the wildfowl reservoir,
612 and which may encode host adaptive changes.
613
614 *Evaluation of viral growth in cell culture*
615 To assess growth, subconfluent cell monolayers in 6 well dishes were inoculated at an MOI of 5
616 PFU/cell (for single-cycle growth assays) or 0.01 PFU/cell (for multi-cycle growth assays) in a
617 200 µl volume. Following incubation for 1 h at 37°C, inocula were removed, cells washed 3x
618 with PBS and 2 ml viral growth medium (MEM (for MDCK cells), DMEM (for 293T, and DF1
619 cells), or F-12K (for A549, and QT-6 cells) medium plus 3% bovine serum albumin, penicillin
620 streptomycin, and TPCK-treated trypsin) was added. Infected cells were incubated at 37°C for
621 the remainder of the time course. At the indicated time points, 120 µl medium was sampled from
622 each dish and 120 µl fresh medium was added to maintain a 2 ml volume. Samples were stored
623 at -80°C and later titered by plaque assay on MDCK cells. Each infection was performed in
624 triplicate and at least three biological replicate infections were carried out on different days. Data
625 are plotted as mean with SD and analyzed by repeated measures ANOVA.
626
627 *Evaluation of viral growth in guinea pigs*
628 Female, Hartley strain, guinea pigs weighing 300-350 g were obtained from Charles River
629 Laboratories. Prior to inoculation or nasal lavage, animals were sedated with a mixture of
630 ketamine (30 mg/kg) and xylazine (4 mg/kg). Virus used for inoculation was diluted in PBS to
631 allow intranasal inoculation of guinea pigs with $1x10^{1}$ to $1x10^{3}$ PFU in a 300 µl volume. Nasal

632 wash samples were collected as described previously [46], with PBS as the collection fluid.
633 Animals were housed in a Caron 6040 environmental chamber set to 10°C and 20% RH
634 throughout the seven-day period and lids were left off of the cages during this time to ensure
635 environmental control within the cages [74].
636
637 *Immunoblotting*
638 A549 or DF-1 cells in 6-well plates were infected with the specified viral strains and cells were
639 lysed with 2X Laemmli sample buffer (Bio-rad) plus 2% beta-mercaptoethanol, 8 hpi. Samples
640 were boiled at 95 ºC for 10 min and resolved on 4-20% gradient SDS-PAGE gels, followed by
641 transfer to nitrocellulose membranes (Bio-rad), and incubation of membranes with 5% non-fat
642 dry milk/TBST blocking buffer. Antibodies used for immunoblotting were: anti-vinculin
643 monoclonal antibody (catalog no. V9131; Sigma-Aldrich) at 1:5000 dilution, IAV nucleoprotein
644 monoclonal antibody (HT-103; catalog no. EMS010, Kerafast) at 1:1000 dilution, IAV matrix
645 protein monoclonal antibody (E10; catalog no. EMS009, Kerafast) at 1:1000 dilution, and LC3B
646 polyclonal antibody (Thermo Fisher Scientific) at 1:1000 dilution. Bands were quantified using
647 ImageLab software (Bio-rad) after normalization to vinculin. At least three biological replicate
648 viral infections were carried out, with two technical replicates of the immunoblotting for each
649 infection. Data shown with error bars representing SD and statistical analysis was carried out
650 using one-way ANOVA with Tukey's multiple comparisons in GraphPad Prism software.
651
652 *Primer extension assay*
653 A549 or DF-1 cells in 6-well plates were infected with the specified viral strains and total RNA
654 was extracted 8 hpi using an RNeasy Kit (Qiagen). Total RNA was eluted in RNase-free water
655 and stored at -80 ºC until needed.
656 Radiolabeling of primers: 1 µmol of oligo DNA primer was incubated with 10 µCuries of ^{32}P-Y-
657 ATP and 10 U of T4 PNK (New England Biolabs) in 70 mM Tris-HCl (pH 7.6) containing 10 mM

658 $MgCl_2$ and 5 mM DTT. Radiolabeling reactions were carried out at 37 ºC for 1 h and diluted to
659 30 µL with RNase-free water after termination of the reaction. Radiolabeled primers were stored
660 at –20 ºC until needed. 500 ng of total RNA was incubated with 0.45 µL unlabeled 5S rRNA
661 primer, 0.05 µL radiolabeled 5S rRNA primer, 0.25 µL radiolabeled IAV segment 7 vRNA
662 primer, and 0.25 µL radiolabeled IAV segment 7 mRNA primer in a final volume of 5 µL. Primers
663 were annealed to RNA by sequential incubations at 95 ºC for 3 min and ice for 3 min. Reactions
664 were pre-warmed at 50 ºC for 5 min. Transcription was initiated by the addition of 50 mM Tris-
665 HCl (pH 8.3) buffer containing 75 mM KCl, 3 mM MgCL2, 10 mM DTT, 2mM dNTP, and 50 units
666 of SuperScript III Reverse Transcriptase (Thermo Fisher Scientific). Reactions were incubated
667 at 50 ºC for 1 h and terminated by the addition of Gel Loading Buffer II (Thermo Fisher
668 Scientific) and incubation at 95 ºC for 10 min. Reactions were resolved on denaturing
669 sequencing polyacrylamide gels (7M urea, 6% acrylamide). Gels were subsequently dried and
670 exposed to a phosphor storage screen overnight. The intensity of bands was analyzed using a
671 Typhoon Trio Imager (GE Healthcare) and quantified with ImageQuant software (GE
672 Healthcare) after normalization to 5S rRNA. At least three biological replicate viral infections
673 were carried out, with two technical replicates of the primer extension assay for each infection.
674 Data are shown with error bars representing SD and statistical analysis was carried out using
675 one-way ANOVA with Tukey's multiple comparisons in GraphPad Prism software.
676
677 *Fluorescence microscopy*
678 To allow tracking of LC3B II and viral protein, cells grown on collagen-coated coverslips were
679 transduced with lentivirus expressing LC3B-GFP (BacMamm 2.0; catalog no. P36235,
680 ThermoFisher), as follows.
681 18h post transduction, 293T or A549 cells were infected with the indicated IAVs at an MOI of 5
682 PFU/cell and incubated at 37°C. At 8h or 12 h post-IAV infection, cells were washed once with
683 PBS and fixed with 4% paraformaldehyde. Following permeabilization with 0.1% Triton X-100,

684 cells were incubated overnight at 4°C with anti-M2 monoclonal antibody (E10; catalog no.
685 EMS009, Kerafast). Three washes were performed prior to addition of goat anti-mouse Alexa
686 Fluor-647 secondary antibody (catalog no. A21241, Life Technologies) and incubation for 2 h at
687 room temperature. Antibody dilutions and washes were performed with PBS plus 1% Tween-20.
688 Cells were treated with DAPI, and coverslips were mounted on slides using Vectashield (Vector
689 Labs) mounting medium. Images were obtained with on an Nikon FV1000 confocal microscope
690 at the Emory Integrated Cellular Imaging core facility.
691
692 *Drug treatments*
693 Where indicated, chloroquine (Invitrogen) was added to cell culture medium at a final
694 concentration of 60 or 120 μM. Amantadine HCl (catalog no. 1018505, Sigma) was added to cell
695 culture medium at a final concentration of 200 μM. Both drugs were added to infected cells 1 h
696 after IAV inoculation.
697
698 *Statistical analyses*
699 Statistical analyses were performed in GraphPad Prism.
700 Multi-cycle and single-cycle growth in cell culture was assessed in three independent
701 experiments, with three technical sample replicates per experiment. Overall statistical
702 significance was determined using repeated measures, two-way, multiple comparisons ANOVA
703 on log transformed mean values, with Bonferroni correction applied to account for comparison
704 of a limited number of means, as well as by assessing pairwise comparisons of viruses at each
705 timepoint, except for single-cycle growth in cell culture in the presence of amantadine, which
706 was assessed in four independent experiments, with three technical sample replicates per
707 experiment. Overall statistical significance was determined using repeated measures, two-way,
708 multiple comparisons ANOVA on log transformed values, with Bonferroni correction applied to

709 account for comparison of a limited number of means, as well as by assessing pairwise
710 comparisons of viruses at each timepoint.
711
712 Growth of each virus in the guinea pig model was assessed in three independent experiments
713 with four guinea pigs per experiment. For transmission analysis, each guinea pig was treated as
714 an independent biological sample. Statistical significance in the magnitude of replication was
715 determined by comparing AUC of growth curves using two-tailed Students t-Test. Statistical
716 significance in transmission efficiency was determined using unpaired two-tailed Students t-
717 Test.
718 Significance of differences in the kinetics of replication was determined by assessing the
719 interaction of time and virus using repeated measures, two-way ANOVA on mean log
720 transformed values, with Bonferroni correction applied to account for comparison of a limited
721 number of means.
722 For experiments presented throughout the manuscript, unless specific values are provided, P
723 values are represented as follows: *< 0.05; **<0.01; ***< 0.001; ****< 0.0001.
724

725 **Acknowledgements**

726 This work was funded by the National Institute of Allergy and Infectious Disease through the
727 Centers of Excellence for Influenza Research and Surveillance (CEIRS) contract no.
728 HHSN272201400004C. We thank Paul Digard for his excellent advice relating to RT Primer
729 Extension assays, and Emory Integrated Cellular Imaging Core Facility for assistance with
730 confocal imaging techniques.
731

732 **Figure Legends**

733 **Figure 1. pH1N1 M segment does not confer improved growth relative to avian M**
734 **segment in avian cells at 37°C. (A)** A panel of PR8-based viruses was rescued by reverse

735 genetics. The viruses differ only in the identity of the M segment, which were derived from
736 A/mallard/MN/99 (H3N8), A/rhea/NC/93 (H7N1), A/duck/Alberta/76 (H1N1), or A/NL/602/09
737 (H1N1) viruses. **(B)** 11-day-old embryonated chicken eggs (ECE) or (C) chicken DF-1 cells
738 were infected at low MOI with the indicated viruses. **(D)** Quail QT-6 cells or **(E)** DF-1 cells were
739 infected at a high MOI of 5 PFU/cell with the indicated viruses. In all avian systems assessed,
740 the pH1N1 M segment did not confer an increase in magnitude or kinetics of growth, relative to
741 any avian-origin M segment. Multi-cycle and single-cycle growth were assessed in three
742 independent experiments, with three technical replicates per experiment. Graphs show the
743 means with SD for the three experiments. Statistical significance was determined using
744 repeated measures, two-way, multiple ANOVA on log transformed values, with Bonferroni
745 correction applied to account for comparison of a limited number of means.
746
747 **Figure 2. pH1N1 M segment confers higher growth relative to avian M segment in**
748 **mammalian cells at 37°C. (A)** canine MDCK cells or **(B)** human A549 cells were inoculated
749 with the indicated viruses at a low MOI of 0.01 PFU/cell. **(C)** MDCK cells or **(D)** A549 cells were
750 inoculated with the indicated viruses at a high MOI of 5 PFU/cell. In mammalian cells, the
751 pH1N1 M segment conferred more rapid kinetics and higher peak titers than any avian-origin M
752 segment. Multi-cycle and single-cycle growth were assessed in three independent experiments,
753 with three technical sample replicates per experiment. Graphs show the means with SD for the
754 three experiments. Statistical significance was determined using repeated measures, two-way,
755 multiple ANOVA on log transformed values, with Bonferroni correction applied to account for
756 comparison of a limited number of means. At each time point, pairwise comparisons between
757 viruses were performed, and asterisks corresponding to the most significant difference observed
758 is shown.
759

760 **Figure 3. pH1N1 influenza A virus M segment confers efficient replication and**
761 **transmission of PR8-based virus among guinea pigs.** Groups of four guinea pigs were
762 inoculated with 10 PFU of each avian M-encoding virus or NL/09 M-encoding virus, as
763 indicated. **(A)** Virus replication in nasal wash was measured by plaque titration at days 2, 4, 6,
764 and 8 post-infection and the area under the curve was calculated. Graphs show mean AUC with
765 SD for three experiments. All avian M-encoding viruses exhibited lower levels of growth in vivo
766 than the isogenic virus possessing the NL/09 M segment. The replication differences between
767 avian M and NL/09 M-based viruses were statistically significant, whereas those among avian
768 M-based viruses were not. Statistical significance was evaluated using an unpaired, two-tailed
769 Student's *t*-test. **(B)** To assess transmission, each inoculated guinea pig was treated as an
770 independent biological sample. The pH1N1 M segment conferred efficient transmission to naïve
771 animals that were contact exposed (7/9 transmissions; 78%). In contrast, significantly poorer
772 (12%), or no transmission was observed from guinea pigs infected with PR8 avian M viruses to
773 naïve cage mates. Statistical significance of transmission differences were evaluated using an
774 unpaired, two-tailed Student's *t*-test.
775
776 **Figure 4. Ratio of M1 to M2 protein expression is high in DF-1 Cells irrespective of viral M**
777 **segment host origin.** DF-1 cells were inoculated at MOI=5, with PR8 viruses encoding the
778 indicated M segments, and incubated at 37°C for 8 hours, then lysed with whole cell lysis buffer.
779 Western blot analysis of virus-infected DF-1 cells: **(A)** Vinculin expression was measured to
780 allow normalization of viral protein levels. NP expression was measured to assess viral
781 replication. Levels of M1 and M2 protein expression were assessed using an antibody (Mab
782 E10) to a common epitope at the amino terminus of M1 and M2 proteins, allowing relative
783 expression to be assessed. Levels of LC3B I and II were assessed using an antibody that
784 detects both the precursor and activated forms of LC3B protein. M1 protein **(B)** and M2 protein
785 **(C)** were normalized to vinculin, quantitated and displayed as a percentage of total protein

786 expressed from the M gene. The ratio of M1:M2 protein expression was calculated and is
787 plotted in **(D).** LC3B I protein **(E)** and LC3B II protein **(F)** were normalized, quantitated and
788 displayed as a percentage of total LC3B protein. Graphs in **B-F** show the means with SD from
789 three independent experiments. For each experiment, two replicate Western blots were
790 performed and quantitated. Statistical significance was assessed using ordinary one-way
791 ANOVA.
792
793 **Figure 5. High expression ratio of M1 to M2 protein in A549 cells is dependent upon viral**
794 **M segment host origin.** A549 cells were inoculated at MOI=5 with PR8 viruses possessing M
795 segments from human or avian host-derived strains and incubated at 37°C for 8 hours, then
796 lysed with whole cell lysis buffer.
797 Western blot analysis of virus-infected A549 cells: **(A)** Vinculin expression was measured to
798 allow normalization of viral protein levels. NP expression was measured to assess viral
799 replication. Levels of M1 and M2 protein expression were assessed using an antibody (Mab
800 E10) to a common epitope at the amino terminus of M1 and M2 proteins, allowing relative
801 expression to be assessed. Levels of LC3B I and II were assessed using an antibody that
802 detects both the precursor and activated forms of LC3B protein. M1 protein **(B)** and M2 protein
803 **(C)** were normalized to vinculin, quantitated and displayed as a percentage of total protein
804 expressed from the M gene. The ratio of M1:M2 protein expression was calculated and is
805 plotted in **(D)**. LC3B I protein **(E)** and LC3B II protein **(F)** were normalized, quantitated and
806 displayed as a percentage of total LC3B protein. Graphs in **B-F** show the means with SD from
807 three independent experiments. For each experiment, two replicate Western blots were
808 performed and quantitated. Statistical significance was assessed using ordinary one-way
809 ANOVA.
810

811 **Figure 6. Ratio of $mRNA_7$ (encoding M1) to $mRNA_{10}$ (encoding M2) expression is high in**
812 **DF-1 cells irrespective of viral M Segment host origin.**
813 DF-1 cells were inoculated at MOI=5 with PR8 viruses encoding the indicated M segments and
814 incubated at 37°C for 8 hours, then lysed with an RNeasy Kit.
815 RT Primer extension radiogram of virus-infected DF-1 cells: **(A)** 5S rRNA levels were measured
816 to allow normalization of viral RNA. Segment 7 vRNA expression was measured to assess viral
817 replication. Levels of $mRNA_7$, $mRNA_{10}$, and $mRNA_{11}$ mRNA expression were assessed using
818 radiolabeled probes. $mRNA_7$ **(B)**, $mRNA_{10}$ **(C)**, and $mRNA_{11}$ **(D)** was quantitated and displayed
819 as a percentage of total M gene expressed mRNA. Graphs in **B-D** show the means with SD
820 from three independent experiments. For each experiment, two replicate radiograms were
821 quantitated. Statistical significance was assessed using ordinary one-way ANOVA.
822
823 **Figure 7. Ratio of $mRNA_7$ (encoding M1) to $mRNA_{10}$ (encoding M2) expression in A549**
824 **cells is dependent upon viral M segment host origin.** A549 cells were inoculated at MOI=5
825 with PR8 viruses encoding the indicated M segments and incubated at 37°C for 8 h prior to RNA
826 extraction. RT Primer extension radiogram of virus-infected A549 cells: **(A)** 5S rRNA levels were
827 measured to allow normalization of viral RNA. Segment 7 vRNA expression was measured to
828 assess viral replication. Levels of $mRNA_7$, $mRNA_{10}$, and $mRNA_{11}$ mRNA expression were
829 assessed using radiolabeled probes. $mRNA_7$ **(B)**, $mRNA_{10}$ **(C)**, and $mRNA_{11}$ **(D)** was
830 quantitated and displayed as a percentage of total M gene expressed mRNA. Graphs in **B-D**
831 show the means with SD from three independent experiments. For each experiment, two
832 replicate radiograms were quantitated. Statistical significance was assessed using ordinary one-
833 way ANOVA.
834
835 **Figure 8. In human cells, avian M2 was expressed at higher levels and localized more**
836 **strongly to perinuclear bodies than human M2.** A549 and 293T cells were inoculated with

837 the indicated viruses, encoding avian or human M segments, at an MOI of 5 PFU/cell. At 8 hpi
838 cells were stained with anti-M2 (Mab E10; red) and DAPI (blue) and imaged by confocal
839 microscopy. Examples of optical sections are shown, either as merged 2-color images or the
840 red and blue channels alone (shown in grey scale). **(A)** A549 cells with 63x magnification. **(B)** 3x
841 magnification of the same images shown in **A**. **(C)** 293T cells with 63x magnification. **(D)** 3x
842 magnification of the same images shown in **C**. Brightness was adjusted for optimal clarity, with
843 all images treated equally.
844
845 **Figure 9. Visualization of LC3 and M2 co-localization.**
846 293T cells were transduced with GFP-LC3 protein and inoculated 24 h later with the indicated
847 IAVs, encoding avian or human-derived M segments, at an MOI of 5 PFU/cell. Cells were fixed
848 8 h later and stained with anti-M2 (Mab E10; red) and DAPI (blue) followed by imaging with
849 confocal microscopy. Examples of optical sections are shown, either as merged 3-color images
850 or the red, green, and blue channels alone (in grey scale). **(A)** 293T cells with 63x magnification.
851 **(B)** 3x magnification of the same images shown in **A**. Brightness was adjusted for optimal
852 clarity, with all images treated equally.
853
854 **Figure 10. Inhibition of M2 ion channel results in loss of activation of LC3B.**
855 A549 cells were inoculated at an MOI=5 PFU/cell with PR8 viruses encoding avian or human-
856 derived M segments and incubated in the presence or absence of 200 μM amantadine from 1
857 hpi. Cells were lysed at 8 hpi. **(A)** Representative Western blot. Vinculin expression was
858 measured to allow normalization of viral protein levels. NP expression was measured to assess
859 viral replication. Levels of M1 and M2 protein were assessed using an antibody (Mab E10) to a
860 common epitope of M1 and M2 proteins, allowing relative expression to be assessed. Levels of
861 LC3B I and II were assessed using an antibody that detects both the precursor and activated
862 forms of LC3B protein. **(B)** M1 protein and **(C)** M2 protein were normalized to vinculin and

863 displayed as a percentage of total M gene expressed protein. **(D)** The ratio of M1:M2 protein
864 expression was calculated. **(E)** LC3B I and **(F)** LC3B II were normalized to vinculin and
865 displayed as a percentage of total LC3B protein. As a control to ensure the specificity of
866 amantadine, we incubated chloroquine-treated A549 cells in the presence or absence of 200
867 μM amantadine for 8 h **(G)**. LC3B I **(H)** and LC3B II **(I)** were normalized to vinculin and
868 displayed as a percentage of total LC3B protein. Graphs in **B-F, H-I** show the means with SD
869 from three independent experiments. For each experiment, two replicate Western blots were
870 performed and quantitated. Statistical significance was assessed using ordinary one-way
871 ANOVA.
872
873 **Figure 11. Inhibition of proton channel activity relieves M2-induced accumulation of LC3B**
874 **positive vesicles.** 293T cells transduced with LC3-GFP were inoculated at MOI=5 PFU/cell with
875 PR8 viruses possessing M segments from a human or an avian strain and incubated in the
876 presence or absence of 200 μM amantadine from 1 hpi. Cells were fixed at 12 hpi and stained
877 with anti-M2 (Mab E10; red) and DAPI (blue) followed by imaging with confocal microscopy.
878 Examples of optical sections are shown, either as merged 3-color images or the red, green, and
879 blue channels alone (in grey scale). 3x zoom of a 63x magnification is shown. Brightness was
880 adjusted for optimal clarity, with all images treated equally.
881
882 **Figure 12. Amantadine improves growth of avian M segment-encoding virus in A549**
883 **cells. Figure 12. Amantadine improves growth of avian M segment-encoding virus in**
884 **A549 Cells at 37°C.**
885 PR8-based NL09 M or Avian M-encoding viruses were inoculated at an MOI of 5 onto A549
886 cells. At 1hpi, cells were treated with 200μM amantadine, and incubated at 37°C for 24 hours in
887 the continuous presence of amantadine. Virus released into supernatant was collected at the

888 indicated time-points, and virus growth was measured by plaque titration. The pH1N1 M
889 segment conferred more rapid kinetics and higher peak titers of growth than the avian-origin M
890 segment, however amantadine had no impact on the growth of the pH1N1 M encoding virus. In
891 contrast, growth of the avian M-encoding virus was improved in the presence of drug (P=
892 0.0007). Single-cycle growth was assessed in four independent experiments, with three
893 technical sample replicates per experiment. Graphs show the means with SD for the four
894 experiments. Statistical significance was determined using repeated measures, two way,
895 multiple comparisons ANOVA on log transformed values, with Sidaks correction applied.
896
897 **Figure 13. Activation of LC3B II correlates with high expression of M2 protein in A549**
898 **cells regardless of M2 amino acid composition.** PR8 NL09 M virus and PR8 Av M virus,
899 along with six chimeric variant PR8-based viruses, were inoculated at an MOI of 5 PFU/cell onto
900 A549 cells. Cells were incubated for 8 h then lysed. **(A)** Western blot analysis of virus-infected
901 A549 cells. Vinculin was measured to allow normalization of viral protein levels. NP was
902 measured to assess viral replication. Levels of M1 and M2 protein were assessed using an
903 antibody (Mab E10) to a common epitope at the amino terminus of M1 and M2 proteins,
904 allowing their direct comparison. Levels of LC3B I and II were assessed using an antibody that
905 detects both the precursor and activated forms of LC3B protein. M1 protein **(B)** and M2 protein
906 **(C)** were normalized to vinculin and displayed as a percentage of total protein expressed from
907 the M gene. **(D)** The ratio of M1:M2 protein is plotted. LC3B I protein **(E)** and LC3B II protein **(F)**
908 were normalized to vinculin and displayed as a percentage of total LC3B protein. Graphs in **B-F**
909 show the means with SD from three independent experiments. For each experiment, two
910 replicate Western blots were performed and quantitated. Statistical significance was assessed
911 using ordinary one-way ANOVA.
912

913 **Figure 14. pH1N1 M amino acid sequences are not sufficient to confer high growth**
914 **phenotype in A549 cells.** PR8 NL09 M virus and PR8 Av M virus, along with six PR8-based
915 viruses carrying avian-human chimeric M segments, were inoculated at an MOI of 5 PFU/cell
916 onto A549 cells. Virus growth was measured by plaque titration. The effects on viral growth of
917 amino acid changes in **(A)** both M1 and M2, **(B)** M1 only and **(C)** M2 only are shown. Single-
918 cycle growth was assessed in at least three independent experiments, with three technical
919 sample replicates per experiment. Graphed data show the means with SD for at least three
920 experiments. Statistical significance was determined using repeated measures, two-way,
921 multiple ANOVA on log transformed values, with Bonferroni correction applied to account for
922 comparison of a limited no of means. Experiments involving PR8 NL09 9mut or 7mut viruses as
923 well as PR8 Av M 9mut or 7mut viruses were performed at the same time, but are displayed on
924 two separate graphs with the same PR8 NL09 M and PR8 Av M control virus data, to improve
925 clarity of presentation.
926 **Figure 15. Reduced expression of avian M2 improves replication efficiency *in vivo* but is**
927 **not sufficient for efficient transmission in guinea pigs.**
928 Groups of twelve guinea pigs were inoculated with 10 PFU of PR8-based viruses carrying avian
929 M, NL09 M, chimeric NL09 M 7mut M, or chimeric avian M 9mut segments, as indicated. **(A)**
930 Virus replication in nasal washings was measured by plaque titration at days 2, 4, 6, and 8 post-
931 infection and the total area under the curve was calculated. The replication differences between
932 viruses encoding the NL09 M 7mut segment and the avian M 9mut segment were statistically
933 significant (P=). Differences between viruses with NL09 M and NL09 M 7mutAv segments, and
934 between avian M and avian M 9mutNL segments were not significant. (**B**) Transmission to
935 naïve cage mates that were exposed at 24 h post inoculation. Neither chimeric M segment
936 conferred efficient transmission (7/9 transmissions; 78%). Statistical significance of replication
937 differences was determined using a two-tailed Students t-Test. Statistical significance of

938 transmission differences was determined using an unpaired two-tailed Students t-Test. NL M
939 and Avian M data are identical to data presented in Figure 3 and are reproduced here for clarity.

940 **References**
941
942 1. Patterson KD, Pyle GF. The geography and mortality of the 1918 influenza pandemic.
943 Bull Hist Med. 1991;65(1):4-21. Epub 1991/01/01. PubMed PMID: 2021692.
944 2. Viboud C, Simonsen L, Fuentes R, Flores J, Miller MA, Chowell G. Global Mortality Impact
945 of the 1957-1959 Influenza Pandemic. J Infect Dis. 2016;213(5):738-45. doi:
946 10.1093/infdis/jiv534. PubMed PMID: 26908781; PubMed Central PMCID: PMC4747626.
947 3. Viboud C, Grais RF, Lafont BA, Miller MA, Simonsen L, Multinational Influenza Seasonal
948 Mortality Study G. Multinational impact of the 1968 Hong Kong influenza pandemic: evidence
949 for a smoldering pandemic. J Infect Dis. 2005;192(2):233-48. doi: 10.1086/431150. PubMed
950 PMID: 15962218.
951 4. Molinari NA, Ortega-Sanchez IR, Messonnier ML, Thompson WW, Wortley PM,
952 Weintraub E, et al. The annual impact of seasonal influenza in the US: measuring disease
953 burden and costs. Vaccine. 2007;25(27):5086-96. Epub 2007/06/05. doi: S0264-410X(07)00385-
954 4 [pii]
955 10.1016/j.vaccine.2007.03.046. PubMed PMID: 17544181.
956 5. Reperant LA, Kuiken T, Osterhaus AD. Adaptive pathways of zoonotic influenza viruses:
957 from exposure to establishment in humans. Vaccine. 2012;30(30):4419-34. Epub 2012/04/28.
958 doi: 10.1016/j.vaccine.2012.04.049
959 S0264-410X(12)00585-3 [pii]. PubMed PMID: 22537992.
960 6. Lowen AC. Constraints, Drivers, and Implications of Influenza A Virus Reassortment.
961 Annual review of virology. 2017. doi: 10.1146/annurev-virology-101416-041726. PubMed
962 PMID: 28548881.
963 7. Steel J, Lowen AC, Mubareka S, Palese P. Transmission of influenza virus in a mammalian
964 host is increased by PB2 amino acids 627K or 627E/701N. PLoS Pathog. 2009;5(1):e1000252.
965 Epub 2009/01/03. doi: 10.1371/journal.ppat.1000252. PubMed PMID: 19119420; PubMed
966 Central PMCID: PMC2603332.
967 8. Subbarao EK, London W, Murphy BR. A single amino acid in the PB2 gene of influenza A
968 virus is a determinant of host range. J Virol. 1993;67(4):1761-4. Epub 1993/04/01. PubMed
969 PMID: 8445709; PubMed Central PMCID: PMC240216.
970 9. Linster M, van Boheemen S, de Graaf M, Schrauwen EJ, Lexmond P, Manz B, et al.
971 Identification, characterization, and natural selection of mutations driving airborne
972 transmission of A/H5N1 virus. Cell. 2014;157(2):329-39. doi: 10.1016/j.cell.2014.02.040.
973 PubMed PMID: 24725402; PubMed Central PMCID: PMC4003409.
974 10. Long JS, Giotis ES, Moncorge O, Frise R, Mistry B, James J, et al. Species difference in
975 ANP32A underlies influenza A virus polymerase host restriction. Nature. 2016;529(7584):101-4.
976 doi: 10.1038/nature16474. PubMed PMID: 26738596; PubMed Central PMCID:
977 PMCPMC4710677.
978 11. Rogers GN, Paulson JC. Receptor determinants of human and animal influenza virus
979 isolates: differences in receptor specificity of the H3 hemagglutinin based on species of origin.
980 Virology. 1983;127(2):361-73. PubMed PMID: 6868370.
981 12. Tanner WD, Toth DJ, Gundlapalli AV. The pandemic potential of avian influenza A(H7N9)
982 virus: a review. Epidemiol Infect. 2015;143(16):3359-74. doi: 10.1017/S0950268815001570.
983 PubMed PMID: 26205078.

984 13. Capua I, Munoz O. Emergence of influenza viruses with zoonotic potential: open issues
985 which need to be addressed. A review. Vet Microbiol. 2013;165(1-2):7-12. doi:
986 10.1016/j.vetmic.2013.01.044. PubMed PMID: 23567150.
987 14. Cauldwell AV, Long JS, Moncorge O, Barclay WS. Viral determinants of influenza A host
988 range. J Gen Virol. 2014. Epub 2014/03/04. doi: 10.1099/vir.0.062836-0
989 vir.0.062836-0 [pii]. PubMed PMID: 24584475.
990 15. Joseph U, Vijaykrishna D, Smith GJD, Su YCF. Adaptive evolution during the
991 establishment of European avian-like H1N1 influenza A virus in swine. Evol Appl.
992 2018;11(4):534-46. doi: 10.1111/eva.12536. PubMed PMID: 29636804; PubMed Central PMCID:
993 PMCPMC5891058.
994 16. Campbell PJ, Danzy S, Kyriakis CS, Deymier MJ, Lowen AC, Steel J. The M segment of the
995 2009 pandemic influenza virus confers increased NA activity, filamentous morphology and
996 efficient contact transmissibility to A/Puerto Rico/8/1934-based reassortant viruses. J Virol.
997 2014. Epub 2014/01/17. doi: JVI.03607-13 [pii]
998 10.1128/JVI.03607-13. PubMed PMID: 24429367.
999 17. Campbell PJ, Kyriakis CS, Marshall N, Suppiah S, Seladi-Schulman J, Danzy S, et al.
1000 Residue 41 of the Eurasian avian-like swine influenza a virus matrix protein modulates virion
1001 filament length and efficiency of contact transmission. J Virol. 2014;88(13):7569-77. Epub
1002 2014/04/25. doi: 10.1128/JVI.00119-14
1003 JVI.00119-14 [pii]. PubMed PMID: 24760887; PubMed Central PMCID: PMC4054412.
1004 18. Seladi-Schulman J, Steel J, Lowen AC. Spherical Influenza Viruses Have a Fitness
1005 Advantage in Embryonated Eggs, while Filament-Producing Strains Are Selected In Vivo. J Virol.
1006 2013;87(24):13343-53. Epub 2013/10/04. doi: 10.1128/JVI.02004-13
1007 JVI.02004-13 [pii]. PubMed PMID: 24089563.
1008 19. Chou YY, Albrecht RA, Pica N, Lowen AC, Richt JA, Garcia-Sastre A, et al. The M segment
1009 of the 2009 new pandemic H1N1 influenza virus is critical for its high transmission efficiency in
1010 the guinea pig model. J Virol. 2011;85(21):11235-41. Epub 2011/09/02. doi: 10.1128/JVI.05794-
1011 11
1012 JVI.05794-11 [pii]. PubMed PMID: 21880744; PubMed Central PMCID: PMC3194962.
1013 20. Lakdawala SS, Lamirande EW, Suguitan AL, Jr., Wang W, Santos CP, Vogel L, et al.
1014 Eurasian-origin gene segments contribute to the transmissibility, aerosol release, and
1015 morphology of the 2009 pandemic H1N1 influenza virus. PLoS Pathog. 2011;7(12):e1002443.
1016 Epub 2012/01/14. doi: 10.1371/journal.ppat.1002443
1017 PPATHOGENS-D-11-01769 [pii]. PubMed PMID: 22241979; PubMed Central PMCID:
1018 PMC3248560.
1019 21. Rossman JS, Lamb RA. Influenza virus assembly and budding. Virology. 2011;411(2):229-
1020 36. Epub 2011/01/18. doi: S0042-6822(10)00747-6 [pii]
1021 10.1016/j.virol.2010.12.003. PubMed PMID: 21237476.
1022 22. Pielak RM, Chou JJ. Flu channel drug resistance: a tale of two sites. Protein Cell.
1023 2010;1(3):246-58. Epub 2011/01/05. doi: 10.1007/s13238-010-0025-y. PubMed PMID:
1024 21203971.
1025 23. Bourmakina SV, Garcia-Sastre A. Reverse genetics studies on the filamentous
1026 morphology of influenza A virus. J Gen Virol. 2003;84(Pt 3):517-27. Epub 2003/02/27. PubMed
1027 PMID: 12604801.

1028 24. Elleman CJ, Barclay WS. The M1 matrix protein controls the filamentous phenotype of
1029 influenza A virus. Virology. 2004;321(1):144-53. Epub 2004/03/23. doi:
1030 10.1016/j.virol.2003.12.009
1031 S0042682204000030 [pii]. PubMed PMID: 15033573.
1032 25. Stauffer S, Feng Y, Nebioglu F, Heilig R, Picotti P, Helenius A. Stepwise priming by acidic
1033 pH and a high K+ concentration is required for efficient uncoating of influenza A virus cores
1034 after penetration. J Virol. 2014;88(22):13029-46. Epub 2014/08/29. doi: 10.1128/JVI.01430-14
1035 JVI.01430-14 [pii]. PubMed PMID: 25165113; PubMed Central PMCID: PMC4249060.
1036 26. O'Neill RE, Talon J, Palese P. The influenza virus NEP (NS2 protein) mediates the nuclear
1037 export of viral ribonucleoproteins. EMBO J. 1998;17(1):288-96. Epub 1998/02/28. doi:
1038 10.1093/emboj/17.1.288. PubMed PMID: 9427762; PubMed Central PMCID: PMC1170379.
1039 27. Akarsu H, Burmeister WP, Petosa C, Petit I, Muller CW, Ruigrok RW, et al. Crystal
1040 structure of the M1 protein-binding domain of the influenza A virus nuclear export protein
1041 (NEP/NS2). EMBO J. 2003;22(18):4646-55. Epub 2003/09/13. doi: 10.1093/emboj/cdg449.
1042 PubMed PMID: 12970177; PubMed Central PMCID: PMC212717.
1043 28. Brunotte L, Flies J, Bolte H, Reuther P, Vreede F, Schwemmle M. The nuclear export
1044 protein of H5N1 influenza A viruses recruits Matrix 1 (M1) protein to the viral ribonucleoprotein
1045 to mediate nuclear export. J Biol Chem. 2014;289(29):20067-77. Epub 2014/06/04. doi:
1046 10.1074/jbc.M114.569178
1047 M114.569178 [pii]. PubMed PMID: 24891509; PubMed Central PMCID: PMC4106323.
1048 29. Watanabe K, Handa H, Mizumoto K, Nagata K. Mechanism for inhibition of influenza
1049 virus RNA polymerase activity by matrix protein. J Virol. 1996;70(1):241-7. Epub 1996/01/01.
1050 PubMed PMID: 8523532; PubMed Central PMCID: PMC189810.
1051 30. Zhang J, Pekosz A, Lamb RA. Influenza virus assembly and lipid raft microdomains: a role
1052 for the cytoplasmic tails of the spike glycoproteins. J Virol. 2000;74(10):4634-44. Epub
1053 2000/04/25. PubMed PMID: 10775599; PubMed Central PMCID: PMC111983.
1054 31. Ali A, Avalos RT, Ponimaskin E, Nayak DP. Influenza virus assembly: effect of influenza
1055 virus glycoproteins on the membrane association of M1 protein. J Virol. 2000;74(18):8709-19.
1056 Epub 2000/08/23. PubMed PMID: 10954572; PubMed Central PMCID: PMC116382.
1057 32. Barman S, Adhikary L, Chakrabarti AK, Bernas C, Kawaoka Y, Nayak DP. Role of
1058 transmembrane domain and cytoplasmic tail amino acid sequences of influenza a virus
1059 neuraminidase in raft association and virus budding. J Virol. 2004;78(10):5258-69. Epub
1060 2004/04/29. PubMed PMID: 15113907; PubMed Central PMCID: PMC400379.
1061 33. Shimbo K, Brassard DL, Lamb RA, Pinto LH. Ion selectivity and activation of the M2 ion
1062 channel of influenza virus. Biophys J. 1996;70(3):1335-46. Epub 1996/03/01. doi: S0006-
1063 3495(96)79690-X [pii]
1064 10.1016/S0006-3495(96)79690-X. PubMed PMID: 8785289; PubMed Central PMCID:
1065 PMC1225059.
1066 34. Grambas S, Hay AJ. Maturation of influenza A virus hemagglutinin--estimates of the pH
1067 encountered during transport and its regulation by the M2 protein. Virology. 1992;190(1):11-8.
1068 Epub 1992/09/01. doi: 0042-6822(92)91187-Y [pii]. PubMed PMID: 1529523.
1069 35. Ciampor F, Thompson CA, Grambas S, Hay AJ. Regulation of pH by the M2 protein of
1070 influenza A viruses. Virus Res. 1992;22(3):247-58. Epub 1992/03/01. PubMed PMID: 1626420.

1071 36. Takeuchi K, Lamb RA. Influenza virus M2 protein ion channel activity stabilizes the native
1072 form of fowl plague virus hemagglutinin during intracellular transport. J Virol. 1994;68(2):911-9.
1073 Epub 1994/02/01. PubMed PMID: 7507186; PubMed Central PMCID: PMC236528.
1074 37. Rossman JS, Jing X, Leser GP, Lamb RA. Influenza virus M2 protein mediates ESCRT-
1075 independent membrane scission. Cell. 2010;142(6):902-13. Epub 2010/09/21. doi: S0092-
1076 8674(10)00960-8 [pii]
1077 10.1016/j.cell.2010.08.029. PubMed PMID: 20850012.
1078 38. Beale R, Wise H, Stuart A, Ravenhill BJ, Digard P, Randow F. A LC3-interacting motif in
1079 the influenza A virus M2 protein is required to subvert autophagy and maintain virion stability.
1080 Cell Host Microbe. 2014;15(2):239-47. doi: 10.1016/j.chom.2014.01.006. PubMed PMID:
1081 24528869; PubMed Central PMCID: PMCPMC3991421.
1082 39. Gannage M, Dormann D, Albrecht R, Dengjel J, Torossi T, Ramer PC, et al. Matrix protein
1083 2 of influenza A virus blocks autophagosome fusion with lysosomes. Cell Host Microbe.
1084 2009;6(4):367-80. Epub 2009/10/20. doi: S1931-3128(09)00314-X [pii]
1085 10.1016/j.chom.2009.09.005. PubMed PMID: 19837376; PubMed Central PMCID:
1086 PMC2774833.
1087 40. Ren Y, Li C, Feng L, Pan W, Li L, Wang Q, et al. Proton Channel Activity of Influenza A
1088 Virus Matrix Protein 2 Contributes to Autophagy Arrest. J Virol. 2016;90(1):591-8. doi:
1089 10.1128/JVI.00576-15. PubMed PMID: 26468520; PubMed Central PMCID: PMCPMC4702553.
1090 41. Kovacs AL, Reith A, Seglen PO. Accumulation of autophagosomes after inhibition of
1091 hepatocytic protein degradation by vinblastine, leupeptin or a lysosomotropic amine. Exp Cell
1092 Res. 1982;137(1):191-201. PubMed PMID: 7056284.
1093 42. Barr JN, Whelan SP, Wertz GW. cis-Acting signals involved in termination of vesicular
1094 stomatitis virus mRNA synthesis include the conserved AUAC and the U7 signal for
1095 polyadenylation. J Virol. 1997;71(11):8718-25. PubMed PMID: 9343230; PubMed Central
1096 PMCID: PMCPMC192336.
1097 43. Barr JN, Whelan SP, Wertz GW. Role of the intergenic dinucleotide in vesicular
1098 stomatitis virus RNA transcription. J Virol. 1997;71(3):1794-801. PubMed PMID: 9032308;
1099 PubMed Central PMCID: PMCPMC191248.
1100 44. Pagan I, Holmes EC, Simon-Loriere E. Level of gene expression is a major determinant of
1101 protein evolution in the viral order Mononegavirales. J Virol. 2012;86(9):5253-63. doi:
1102 10.1128/JVI.06050-11. PubMed PMID: 22345453; PubMed Central PMCID: PMCPMC3347393.
1103 45. Abraham G, Banerjee AK. Sequential transcription of the genes of vesicular stomatitis
1104 virus. Proc Natl Acad Sci U S A. 1976;73(5):1504-8. PubMed PMID: 179088; PubMed Central
1105 PMCID: PMCPMC430325.
1106 46. Lowen AC, Mubareka S, Tumpey TM, Garcia-Sastre A, Palese P. The guinea pig as a
1107 transmission model for human influenza viruses. Proc Natl Acad Sci U S A. 2006;103(26):9988-
1108 92. Epub 2006/06/21. doi: 0604157103 [pii]
1109 10.1073/pnas.0604157103. PubMed PMID: 16785447; PubMed Central PMCID: PMC1502566.
1110 47. Lowen AC, Bouvier NM, Steel J. Transmission in the guinea pig model. Curr Top
1111 Microbiol Immunol. 2014;385:157-83. doi: 10.1007/82_2014_390. PubMed PMID: 25001209.
1112 48. Inglis SC, Brown CM. Spliced and unspliced RNAs encoded by virion RNA segment 7 of
1113 influenza virus. Nucleic Acids Res. 1981;9(12):2727-40. PubMed PMID: 6169001; PubMed
1114 Central PMCID: PMCPMC326888.

1115 49. Lamb RA, Lai CJ, Choppin PW. Sequences of mRNAs derived from genome RNA segment
1116 7 of influenza virus: colinear and interrupted mRNAs code for overlapping proteins. Proc Natl
1117 Acad Sci U S A. 1981;78(7):4170-4. PubMed PMID: 6945577; PubMed Central PMCID:
1118 PMCPMC319750.
1119 50. Inglis SC, Brown CM. Differences in the control of virus mRNA splicing during permissive
1120 or abortive infection with influenza A (fowl plague) virus. J Gen Virol. 1984;65 (Pt 1):153-64.
1121 doi: 10.1099/0022-1317-65-1-153. PubMed PMID: 6546394.
1122 51. Lau SC, Scholtissek C. Abortive infection of Vero cells by an influenza A virus (FPV).
1123 Virology. 1995;212(1):225-31. Epub 1995/09/10. doi: S0042-6822(85)71473-0 [pii]
1124 10.1006/viro.1995.1473. PubMed PMID: 7676635.
1125 52. Fujita N, Itoh T, Omori H, Fukuda M, Noda T, Yoshimori T. The Atg16L complex specifies
1126 the site of LC3 lipidation for membrane biogenesis in autophagy. Mol Biol Cell.
1127 2008;19(5):2092-100. doi: 10.1091/mbc.E07-12-1257. PubMed PMID: 18321988; PubMed
1128 Central PMCID: PMCPMC2366860.
1129 53. Hanada T, Noda NN, Satomi Y, Ichimura Y, Fujioka Y, Takao T, et al. The Atg12-Atg5
1130 conjugate has a novel E3-like activity for protein lipidation in autophagy. J Biol Chem.
1131 2007;282(52):37298-302. doi: 10.1074/jbc.C700195200. PubMed PMID: 17986448.
1132 54. Barth S, Glick D, Macleod KF. Autophagy: assays and artifacts. J Pathol. 2010;221(2):117-
1133 24. doi: 10.1002/path.2694. PubMed PMID: 20225337; PubMed Central PMCID:
1134 PMCPMC2989884.
1135 55. Mauthe M, Orhon I, Rocchi C, Zhou X, Luhr M, Hijlkema KJ, et al. Chloroquine inhibits
1136 autophagic flux by decreasing autophagosome-lysosome fusion. Autophagy. 2018;14(8):1435-
1137 55. doi: 10.1080/15548627.2018.1474314. PubMed PMID: 29940786; PubMed Central PMCID:
1138 PMCPMC6103682.
1139 56. Skehel JJ, Hay AJ, Armstrong JA. On the mechanism of inhibition of influenza virus
1140 replication by amantadine hydrochloride. J Gen Virol. 1978;38(1):97-110. doi: 10.1099/0022-
1141 1317-38-1-97. PubMed PMID: 563896.
1142 57. van Wielink R, Harmsen MM, Martens DE, Peeters BP, Wijffels RH, Moormann RJ.
1143 Mutations in the M-gene segment can substantially increase replication efficiency of NS1
1144 deletion influenza A virus in MDCK cells. J Virol. 2012;86(22):12341-50. doi: 10.1128/JVI.01725-
1145 12. PubMed PMID: 22951840; PubMed Central PMCID: PMCPMC3486480.
1146 58. Spronken MI, van de Sandt CE, de Jongh EP, Vuong O, van der Vliet S, Bestebroer TM, et
1147 al. A compensatory mutagenesis study of a conserved hairpin in the M gene segment of
1148 influenza A virus shows its role in virus replication. RNA Biol. 2017;14(11):1606-16. doi:
1149 10.1080/15476286.2017.1338243. PubMed PMID: 28662365; PubMed Central PMCID:
1150 PMCPMC5785231.
1151 59. Shih SR, Krug RM. Novel exploitation of a nuclear function by influenza virus: the cellular
1152 SF2/ASF splicing factor controls the amount of the essential viral M2 ion channel protein in
1153 infected cells. EMBO J. 1996;15(19):5415-27. PubMed PMID: 8895585; PubMed Central PMCID:
1154 PMCPMC452284.
1155 60. Thompson MG, Munoz-Moreno R, Bhat P, Roytenberg R, Lindberg J, Gazzara MR, et al.
1156 Co-regulatory activity of hnRNP K and NS1-BP in influenza and human mRNA splicing. Nat
1157 Commun. 2018;9(1):2407. doi: 10.1038/s41467-018-04779-4. PubMed PMID: 29921878;
1158 PubMed Central PMCID: PMCPMC6008300.

1159 61. Ren Y, Li C, Feng L, Pan W, Li L, Wang Q, et al. Proton Channel Activity of Influenza A
1160 Virus Matrix Protein 2 Contributes to Autophagy Arrest. J Virol. 2015;90(1):591-8. doi:
1161 10.1128/JVI.00576-15. PubMed PMID: 26468520; PubMed Central PMCID: PMCPMC4702553.
1162 62. Zhirnov OP, Klenk HD. Influenza A virus proteins NS1 and hemagglutinin along with M2
1163 are involved in stimulation of autophagy in infected cells. J Virol. 2013;87(24):13107-14. doi:
1164 10.1128/JVI.02148-13. PubMed PMID: 24027311; PubMed Central PMCID: PMCPMC3838240.
1165 63. Heaton NS, Randall G. Dengue virus and autophagy. Viruses. 2011;3(8):1332-41. doi:
1166 10.3390/v3081332. PubMed PMID: 21994782; PubMed Central PMCID: PMCPMC3185800.
1167 64. Heaton NS, Randall G. Dengue virus-induced autophagy regulates lipid metabolism. Cell
1168 Host Microbe. 2010;8(5):422-32. doi: 10.1016/j.chom.2010.10.006. PubMed PMID: 21075353;
1169 PubMed Central PMCID: PMCPMC3026642.
1170 65. Zhang J, Lan Y, Li MY, Lamers MM, Fusade-Boyer M, Klemm E, et al. Flaviviruses Exploit
1171 the Lipid Droplet Protein AUP1 to Trigger Lipophagy and Drive Virus Production. Cell Host
1172 Microbe. 2018;23(6):819-31 e5. doi: 10.1016/j.chom.2018.05.005. PubMed PMID: 29902443.
1173 66. Henkel JR, Weisz OA. Influenza virus M2 protein slows traffic along the secretory
1174 pathway. pH perturbation of acidified compartments affects early Golgi transport steps. J Biol
1175 Chem. 1998;273(11):6518-24. PubMed PMID: 9497387.
1176 67. Henkel JR, Apodaca G, Altschuler Y, Hardy S, Weisz OA. Selective perturbation of apical
1177 membrane traffic by expression of influenza M2, an acid-activated ion channel, in polarized
1178 madin-darby canine kidney cells. Mol Biol Cell. 1998;9(9):2477-90. PubMed PMID: 9725907;
1179 PubMed Central PMCID: PMCPMC25516.
1180 68. Henkel JR, Popovich JL, Gibson GA, Watkins SC, Weisz OA. Selective perturbation of early
1181 endosome and/or trans-Golgi network pH but not lysosome pH by dose-dependent expression
1182 of influenza M2 protein. J Biol Chem. 1999;274(14):9854-60. PubMed PMID: 10092677.
1183 69. Burleigh LM, Calder LJ, Skehel JJ, Steinhauer DA. Influenza a viruses with mutations in
1184 the m1 helix six domain display a wide variety of morphological phenotypes. J Virol.
1185 2005;79(2):1262-70. Epub 2004/12/23. doi: 79/2/1262 [pii]
1186 10.1128/JVI.79.2.1262-1270.2005. PubMed PMID: 15613353; PubMed Central PMCID:
1187 PMC538569.
1188 70. Roberts PC, Lamb RA, Compans RW. The M1 and M2 proteins of influenza A virus are
1189 important determinants in filamentous particle formation. Virology. 1998;240(1):127-37. Epub
1190 1998/02/04. doi: S0042-6822(97)98916-9 [pii]
1191 10.1006/viro.1997.8916. PubMed PMID: 9448697.
1192 71. Fodor E, Devenish L, Engelhardt OG, Palese P, Brownlee GG, Garcia-Sastre A. Rescue of
1193 influenza A virus from recombinant DNA. J Virol. 1999;73(11):9679-82. Epub 1999/10/09.
1194 PubMed PMID: 10516084; PubMed Central PMCID: PMCPmc113010.
1195 72. Chutinimitkul S, Herfst S, Steel J, Lowen AC, Ye J, van Riel D, et al. Virulence-Associated
1196 Substitution D222G in the Hemagglutinin of 2009 Pandemic Influenza A(H1N1) Virus Affects
1197 Receptor Binding. J Virol. 2010;84(22):11802-13. doi: 10.1128/JVI.01136-10. PubMed PMID:
1198 PMC2977876.
1199 73. Quinlivan M, Zamarin D, Garcia-Sastre A, Cullinane A, Chambers T, Palese P. Attenuation
1200 of equine influenza viruses through truncations of the NS1 protein. J Virol. 2005;79(13):8431-9.
1201 Epub 2005/06/16. doi: 79/13/8431 [pii]

1202 10.1128/JVI.79.13.8431-8439.2005. PubMed PMID: 15956587; PubMed Central PMCID:
1203 PMC1143746.
1204 74. Lowen AC, Mubareka S, Steel J, Palese P. Influenza virus transmission is dependent on
1205 relative humidity and temperature. PLoS Pathog. 2007;3(10):1470-6. Epub 2007/10/24. doi: 07-
1206 PLPA-RA-0426 [pii]
1207 10.1371/journal.ppat.0030151. PubMed PMID: 17953482; PubMed Central PMCID:
1208 PMC2034399.
1209

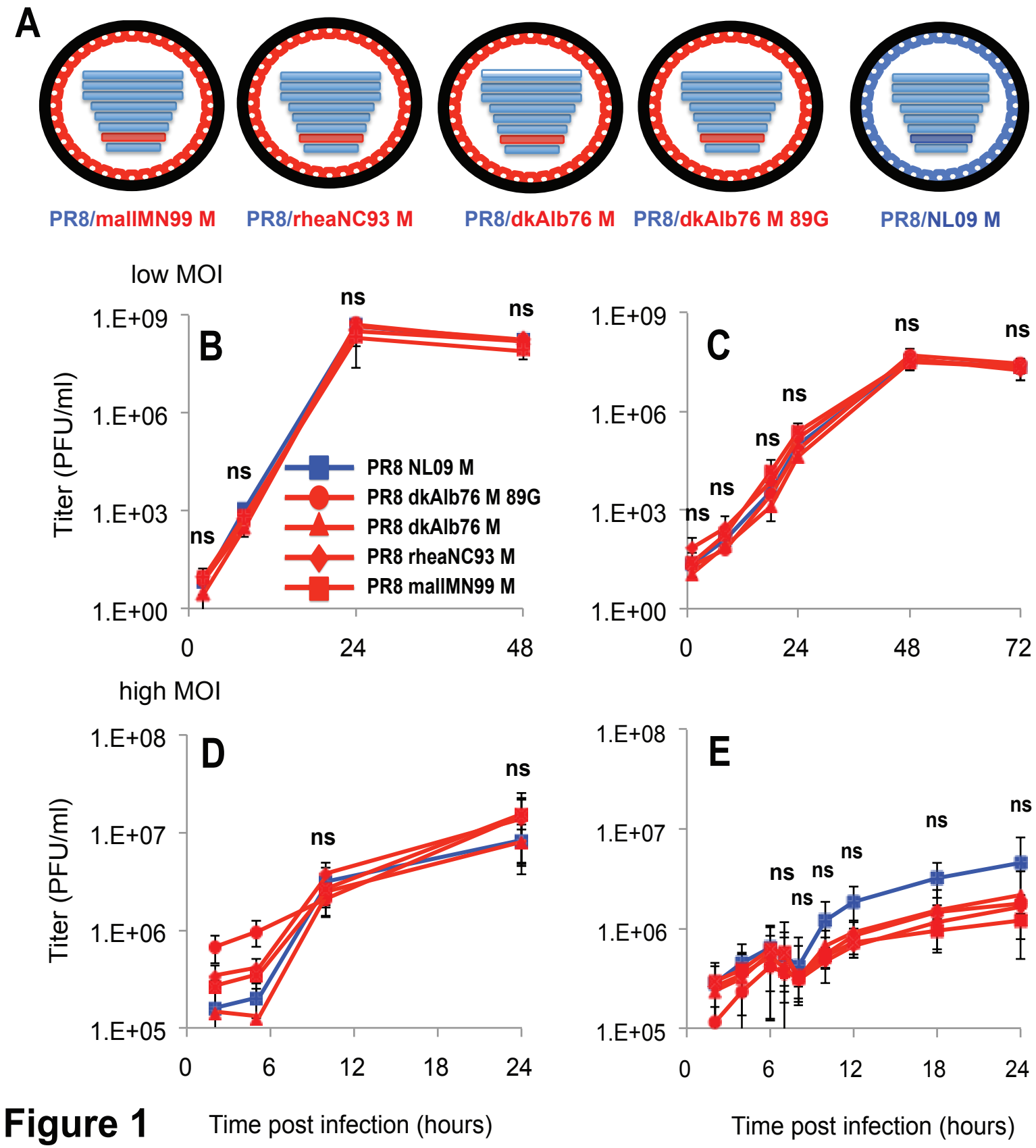
A
PR8/mallMN99 M
PR8/rheaNC93 M
PR8/dkAlb76 M
PR8/dkAlb76 M 89G
PR8/NL09 M
low MOI
B
C
Titer (PFU/ml)
1.E+09
1.E+06
1.E+03
1.E+00
0
24
48
72
ns
PR8 NL09 M
PR8 dkAlb76 M 89G
PR8 dkAlb76 M
PR8 rheaNC93 M
PR8 mallMN99 M
high MOI
D
E
1.E+08
1.E+07
1.E+05
6
12
18
Time post infection (hours)

Figure 1

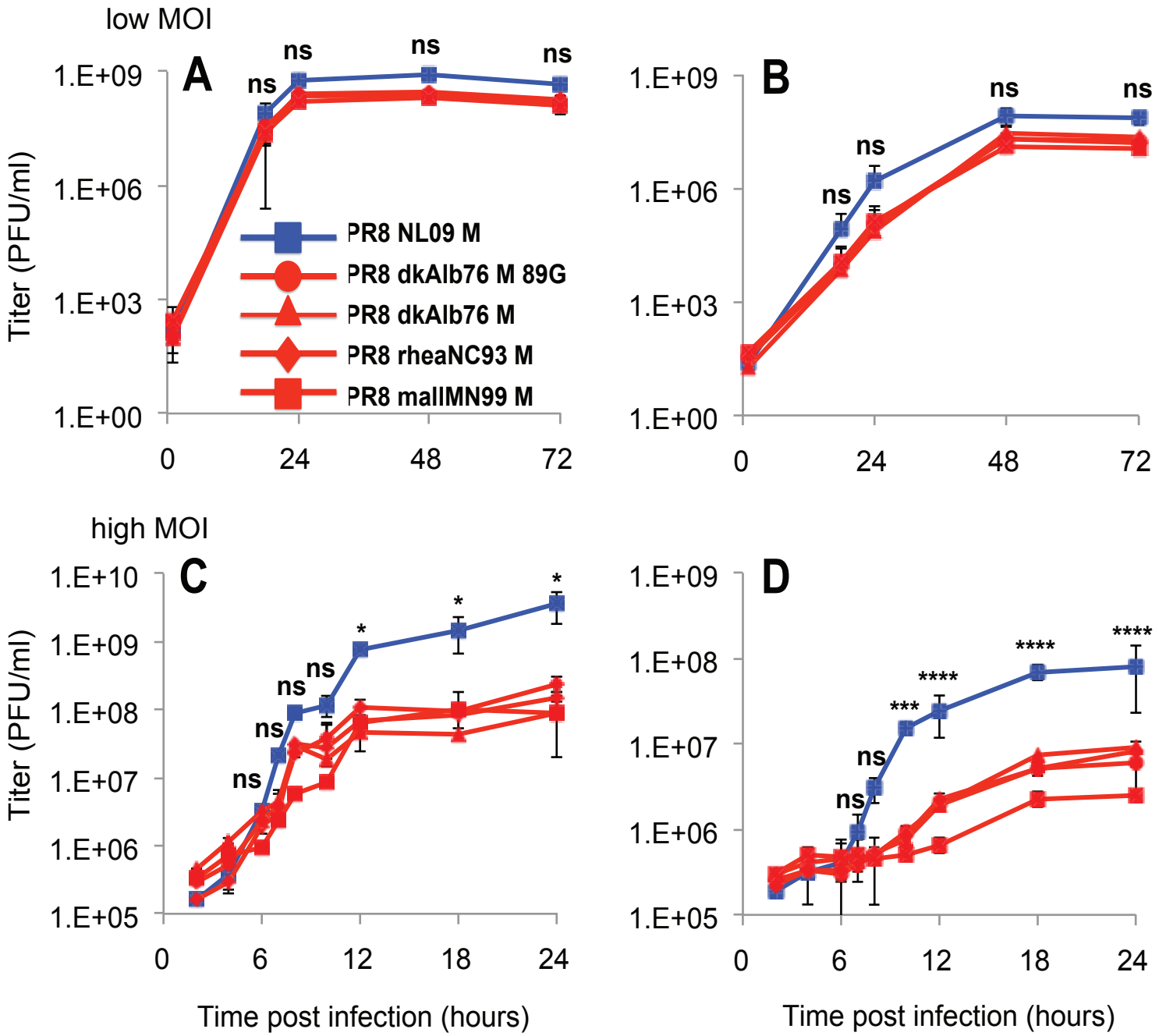
low MOI
A
B
high MOI
C
D
Titer (PFU/ml)
1.E+09
1.E+06
1.E+03
1.E+00
1.E+10
1.E+08
1.E+07
1.E+05
0
24
48
72
6
12
18
ns
*
***
****
PR8 NL09 M
PR8 dkAlb76 M 89G
PR8 dkAlb76 M
PR8 rheaNC93 M
PR8 mallMN99 M
Time post infection (hours)

Figure 2

Figure 3

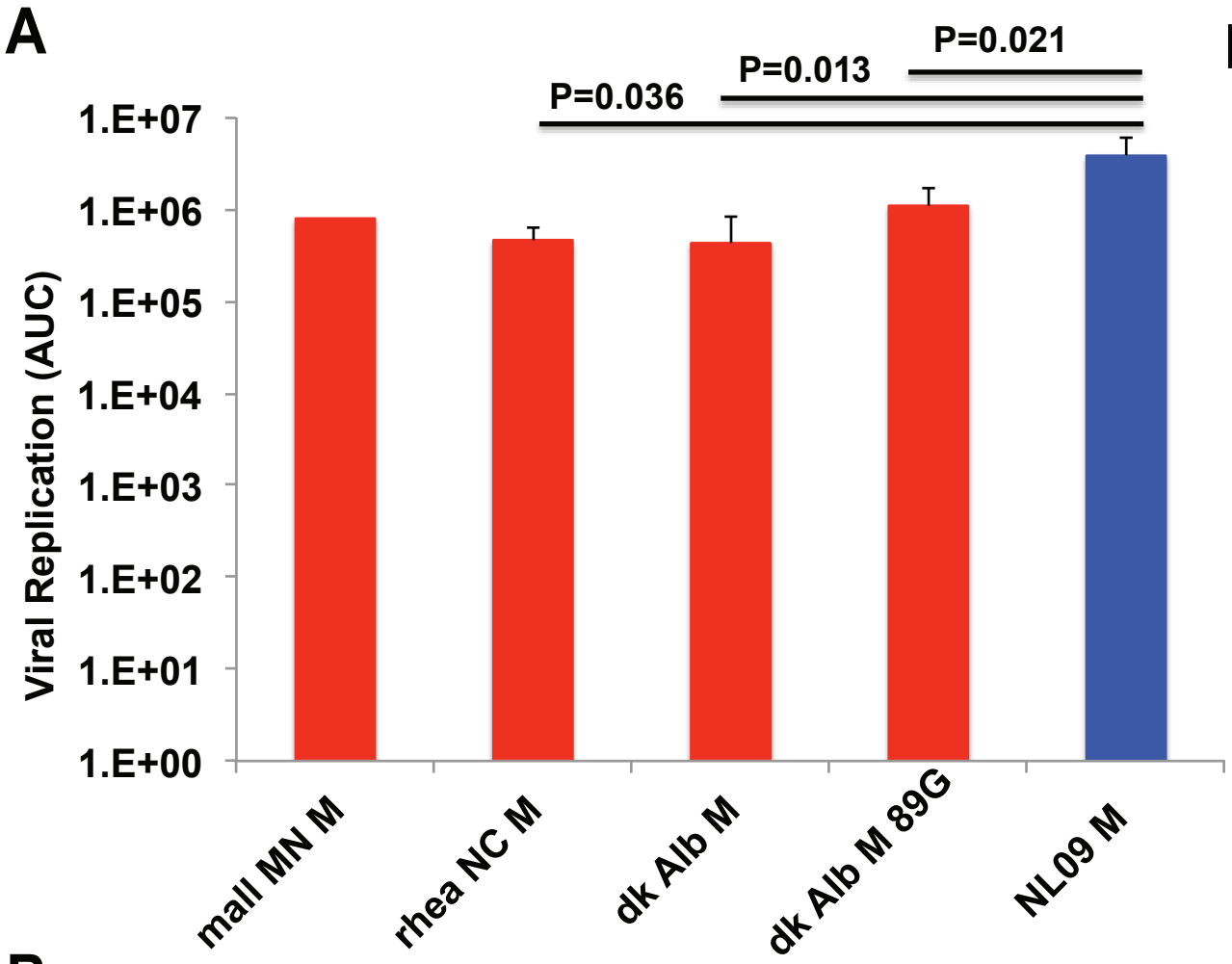
A
P=0.036
P=0.013
P=0.021
Viral Replication (AUC)
1.E+07
1.E+06
1.E+05
1.E+04
1.E+03
1.E+02
1.E+01
1.E+00
mall MN M
rhea NC M
dk Alb M
dk Alb M 89G
NL09 M

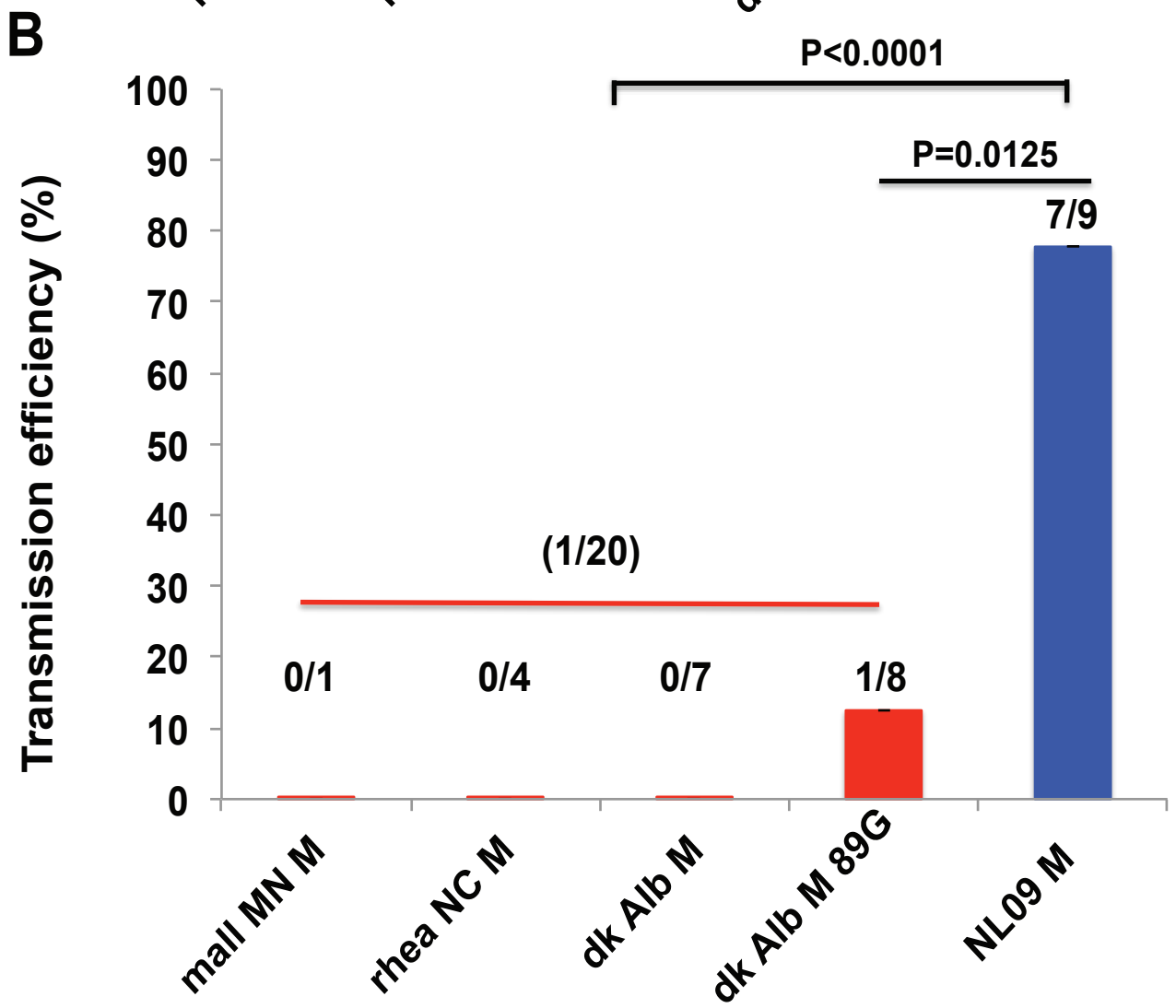
B
P<0.0001
P=0.0125
Transmission efficiency (%)
100
90
80
70
60
50
40
30
20
10
0
(1/20)
0/1
0/4
0/7
1/8
7/9
mall MN M
rhea NC M
dk Alb M
dk Alb M 89G
NL09 M

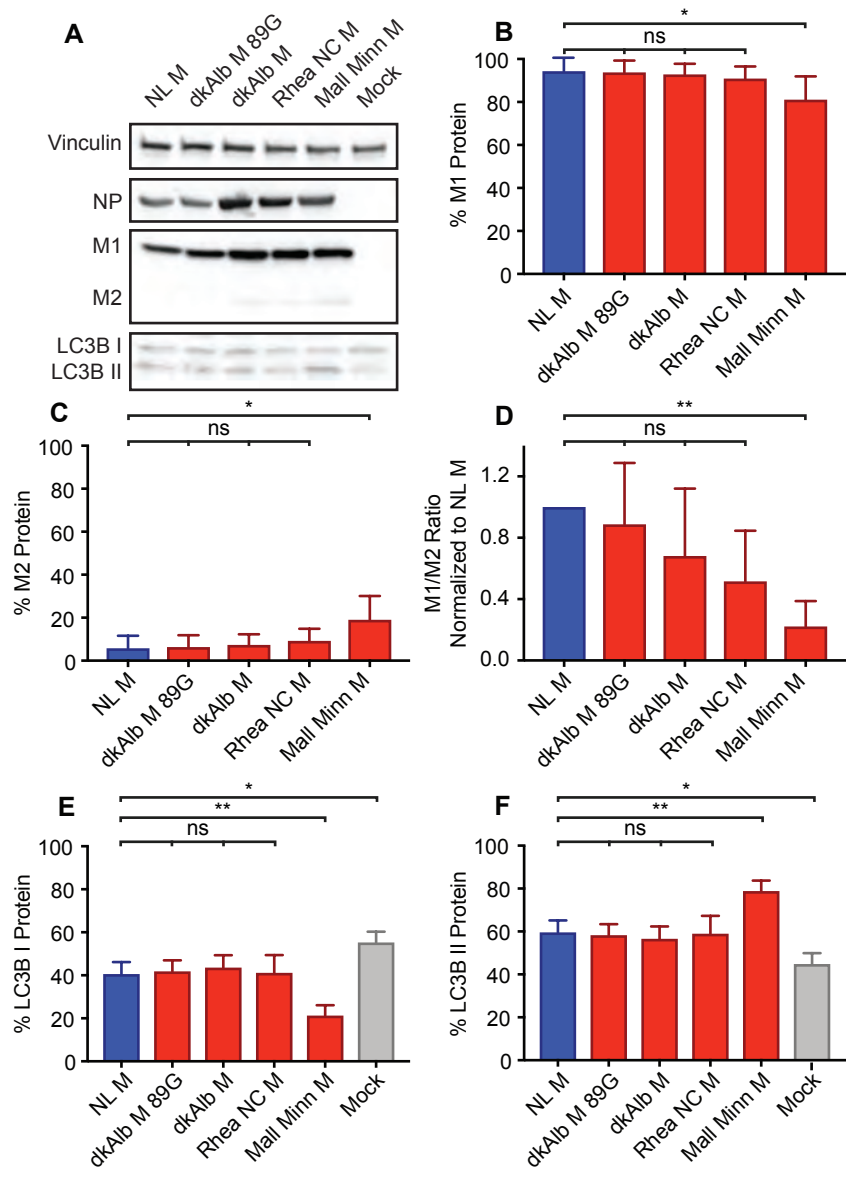
A
NL M
dkAlb M 89G
dkAlb M
Rhea NC M
Mall Minn M
Mock
Vinculin
NP
M1
M2
LC3B I
LC3B II
B
% M1 Protein
ns
*
C
% M2 Protein
ns
*
D
M1/M2 Ratio
Normalized to NL M
ns
**
E
% LC3B I Protein
ns
**
*
F
% LC3B II Protein
ns
**
*

Figure 4

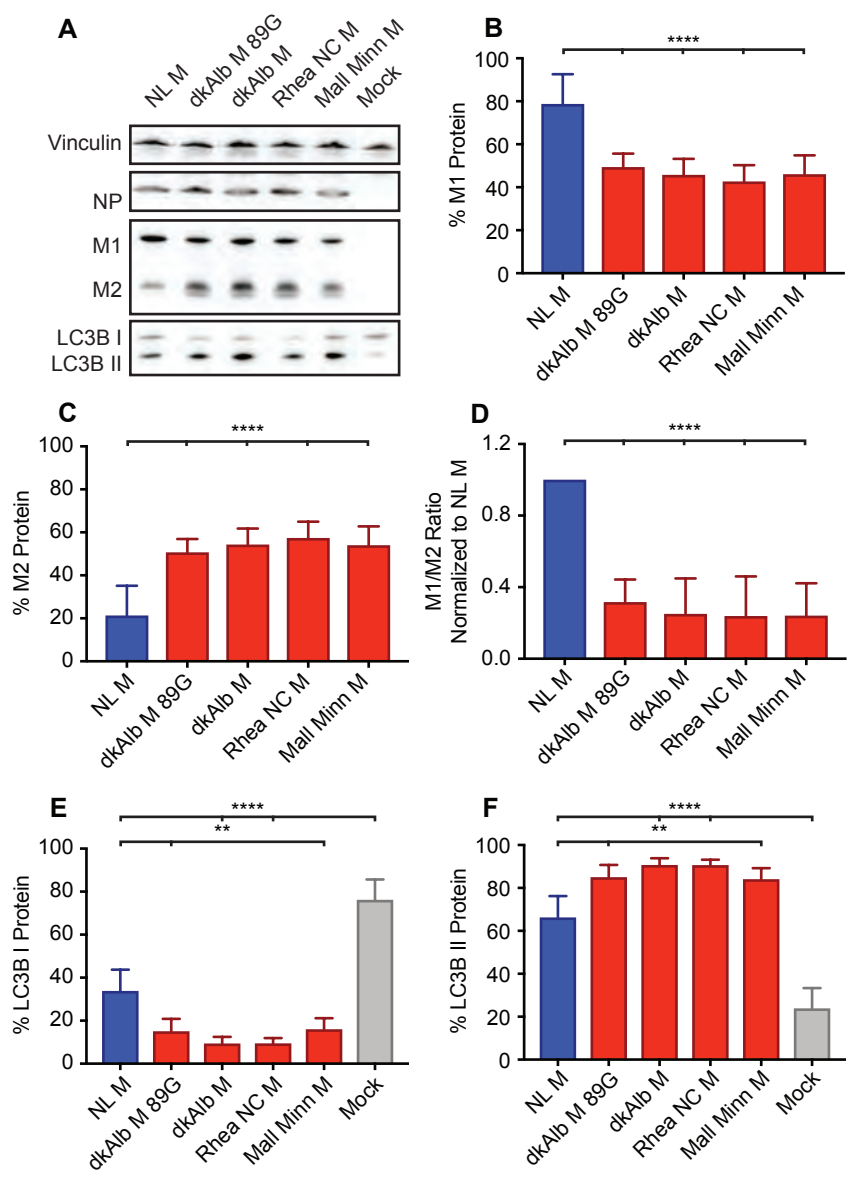
A
NL M
dkAlb M 89G
dkAlb M
Rhea NC M
Mall Minn M
Mock
Vinculin
NP
M1
M2
LC3B I
LC3B II
B
% M1 Protein
****
C
% M2 Protein
****
D
M1/M2 Ratio
Normalized to NL M
****
E
% LC3B I Protein
****
**
F
% LC3B II Protein
****
**

Figure 5

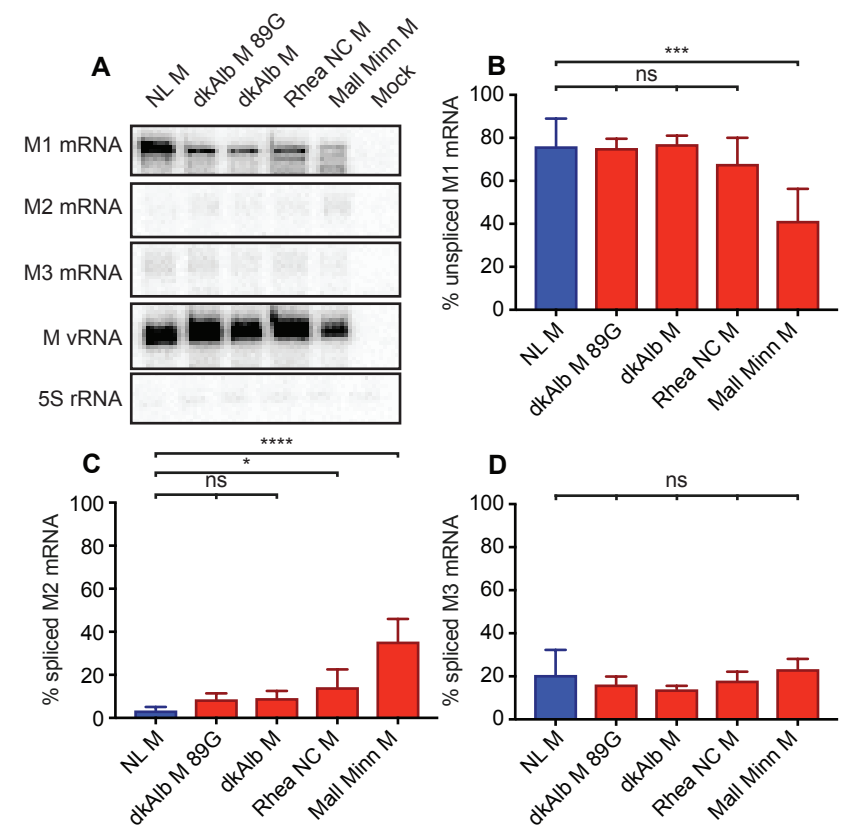
A
NL M
dkAlb M 89G
dkAlb M
Rhea NC M
Mall Minn M
Mock
M1 mRNA
M2 mRNA
M3 mRNA
M vRNA
5S rRNA
B
***
ns
% unspliced M1 mRNA
100
80
60
40
20
0
NL M
dkAlb M 89G
dkAlb M
Rhea NC M
Mall Minn M
C
****
*
ns
% spliced M2 mRNA
100
80
60
40
20
0
NL M
dkAlb M 89G
dkAlb M
Rhea NC M
Mall Minn M
D
ns
% spliced M3 mRNA
100
80
60
40
20
0
NL M
dkAlb M 89G
dkAlb M
Rhea NC M
Mall Minn M

Figure 6

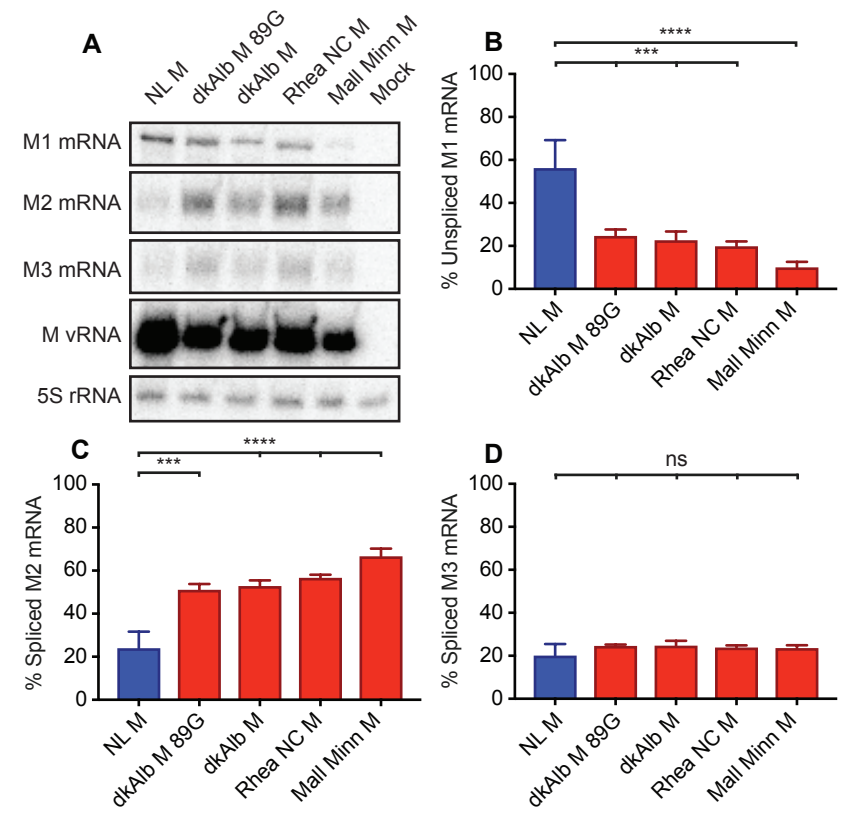
A
NL M
dkAlb M 89G
dkAlb M
Rhea NC M
Mall Minn M
Mock
M1 mRNA
M2 mRNA
M3 mRNA
M vRNA
5S rRNA
B
****
***
% Unspliced M1 mRNA
100
80
60
40
20
0
NL M
dkAlb M 89G
dkAlb M
Rhea NC M
Mall Minn M
C
***
****
% Spliced M2 mRNA
100
80
60
40
20
0
NL M
dkAlb M 89G
dkAlb M
Rhea NC M
Mall Minn M
D
ns
% Spliced M3 mRNA
100
80
60
40
20
0
NL M
dkAlb M 89G
dkAlb M
Rhea NC M
Mall Minn M

Figure 7

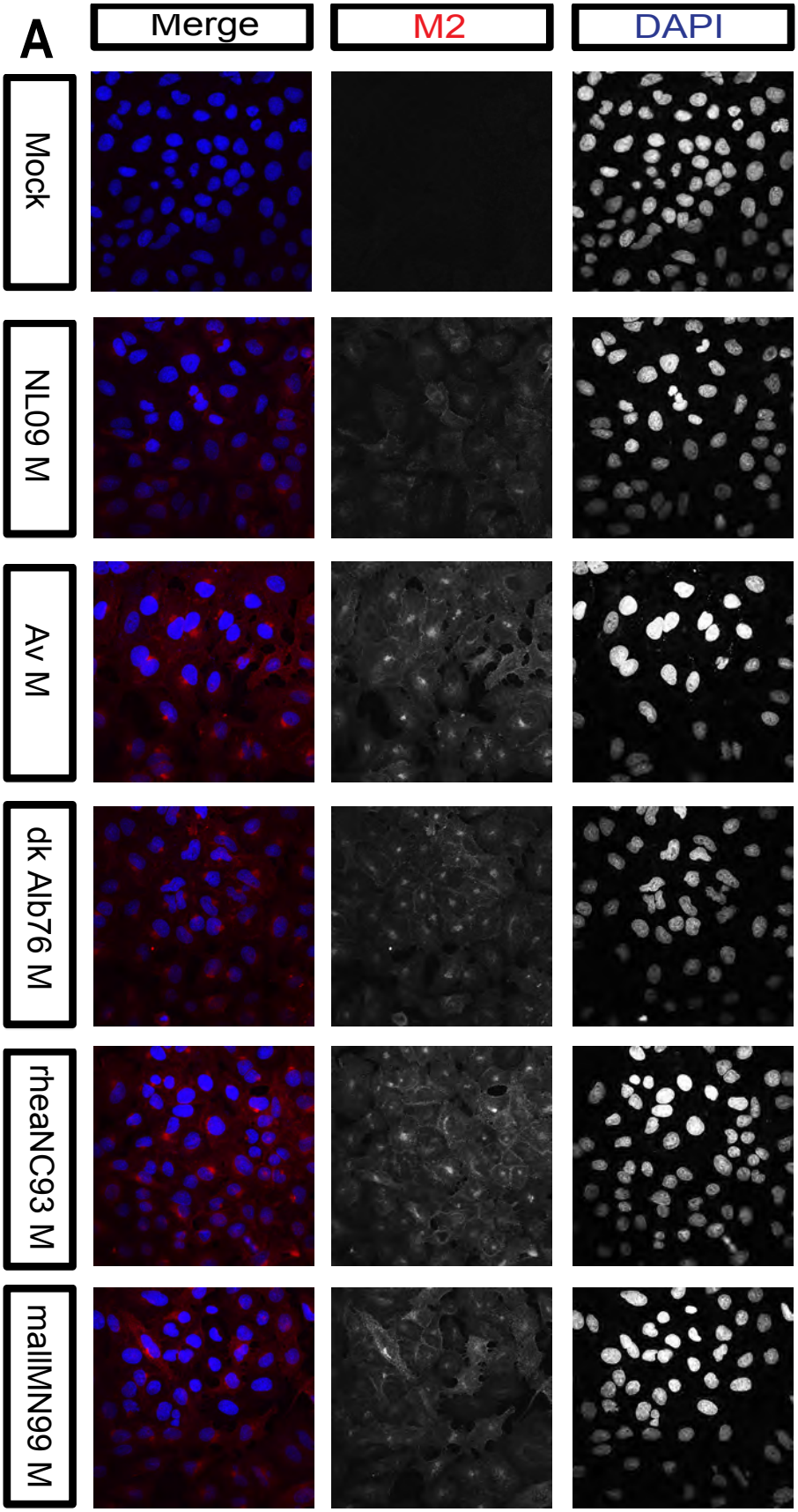
A
Merge
M2
DAPI
Mock
NL09 M
Av M
dk Alb76 M
rheaNC93 M
mallMN99 M

Figure 8

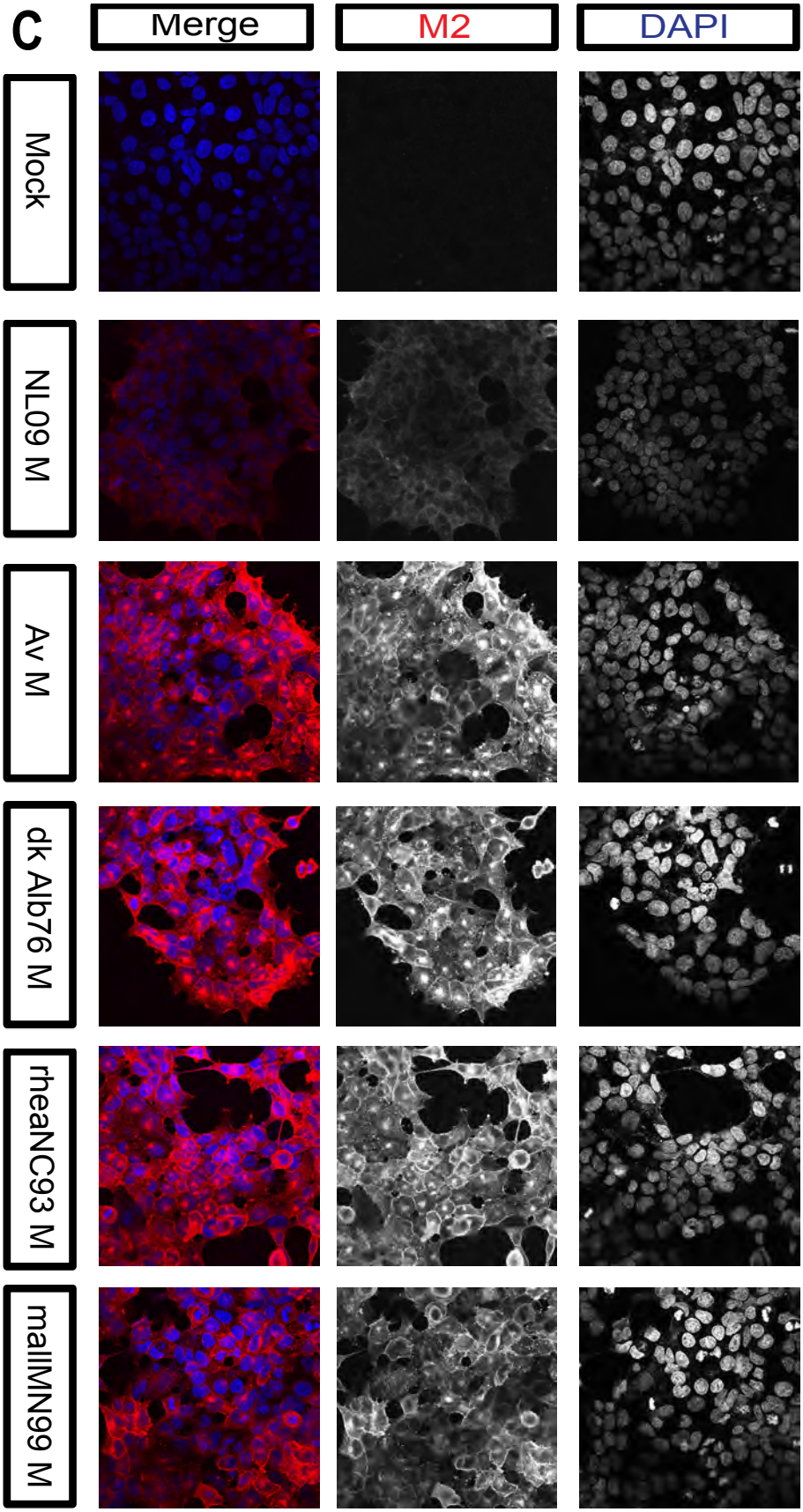

Figure 8 contd

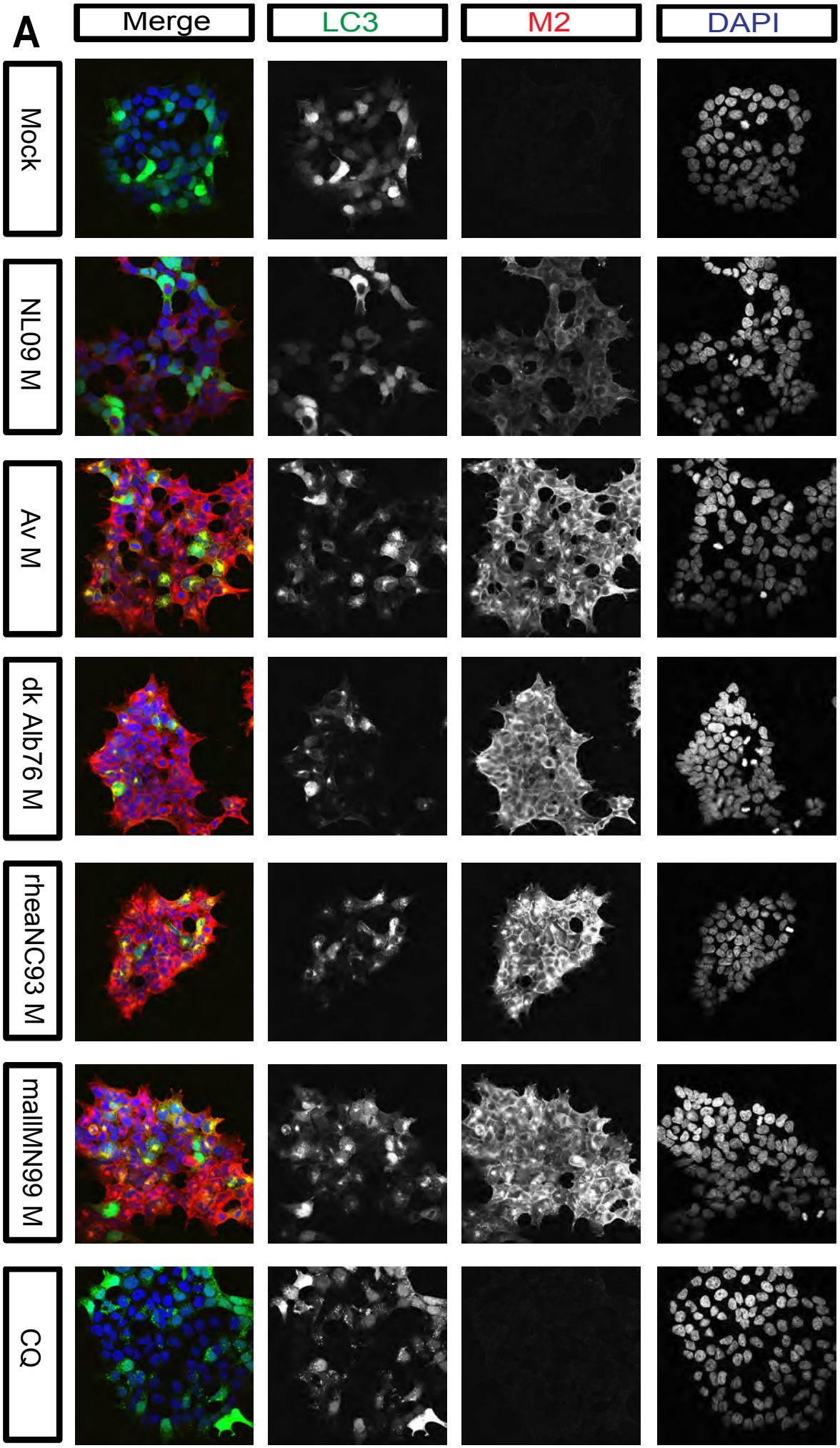
A
Merge
LC3
M2
DAPI
Mock
NL09 M
Av M
dk Alb76 M
rheaNC93 M
mallMN99 M
CQ

Figure 9

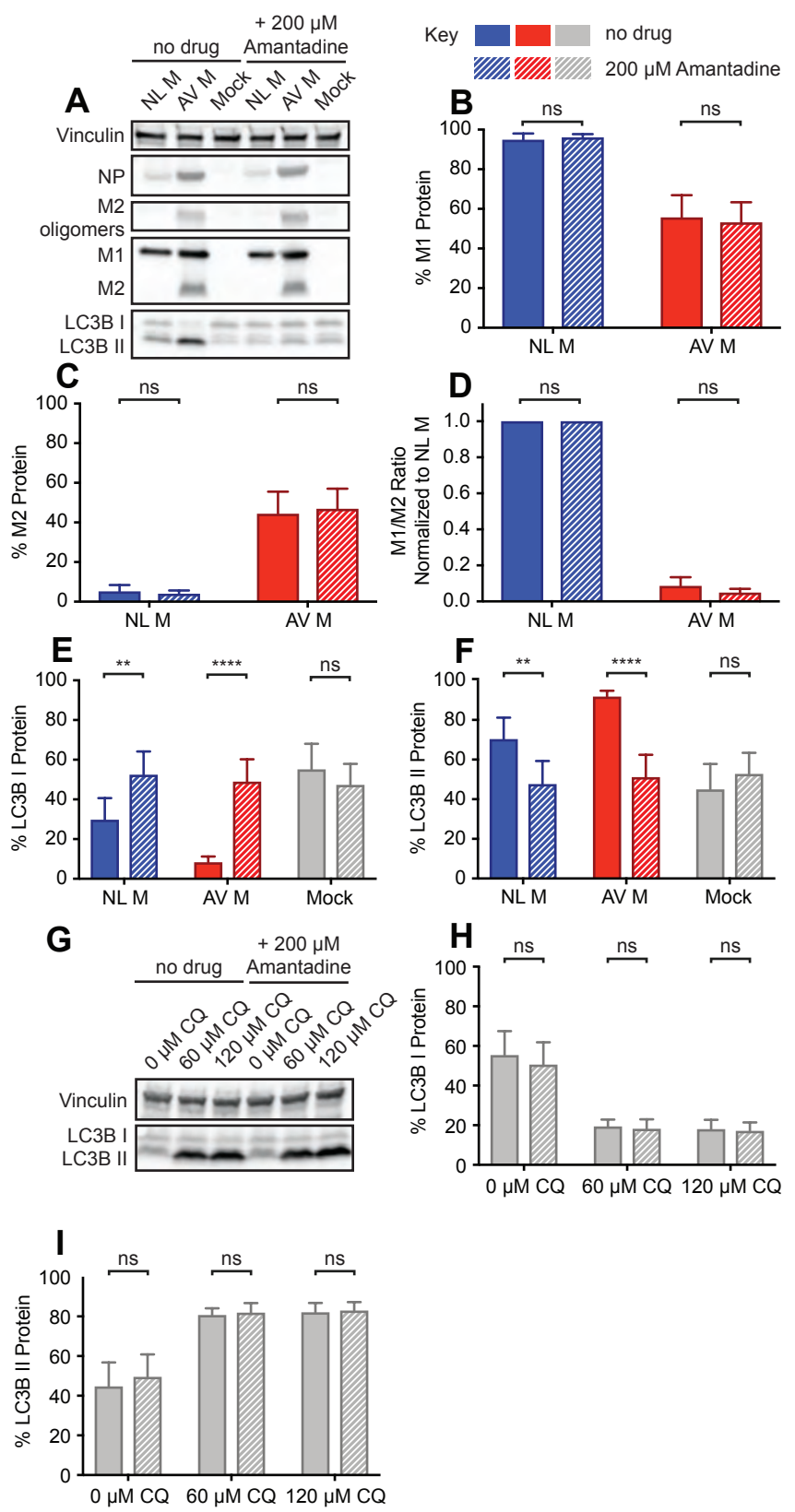
A
no drug
+ 200 μM Amantadine
NL M
AV M
Mock
NL M
AV M
Mock
Vinculin
NP
M2 oligomers
M1
M2
LC3B I
LC3B II
Key
no drug
200 μM Amantadine
B
% M1 Protein
ns
ns
NL M
AV M
C
% M2 Protein
ns
ns
NL M
AV M
D
M1/M2 Ratio Normalized to NL M
ns
ns
NL M
AV M
E
% LC3B I Protein
**
****
ns
NL M
AV M
Mock
F
% LC3B II Protein
**
****
ns
NL M
AV M
Mock
G
no drug
+ 200 μM Amantadine
0 μM CQ
60 μM CQ
120 μM CQ
0 μM CQ
60 μM CQ
120 μM CQ
Vinculin
LC3B I
LC3B II
H
% LC3B I Protein
ns
ns
ns
0 μM CQ
60 μM CQ
120 μM CQ
I
% LC3B II Protein
ns
ns
ns
0 μM CQ
60 μM CQ
120 μM CQ

Figure 10

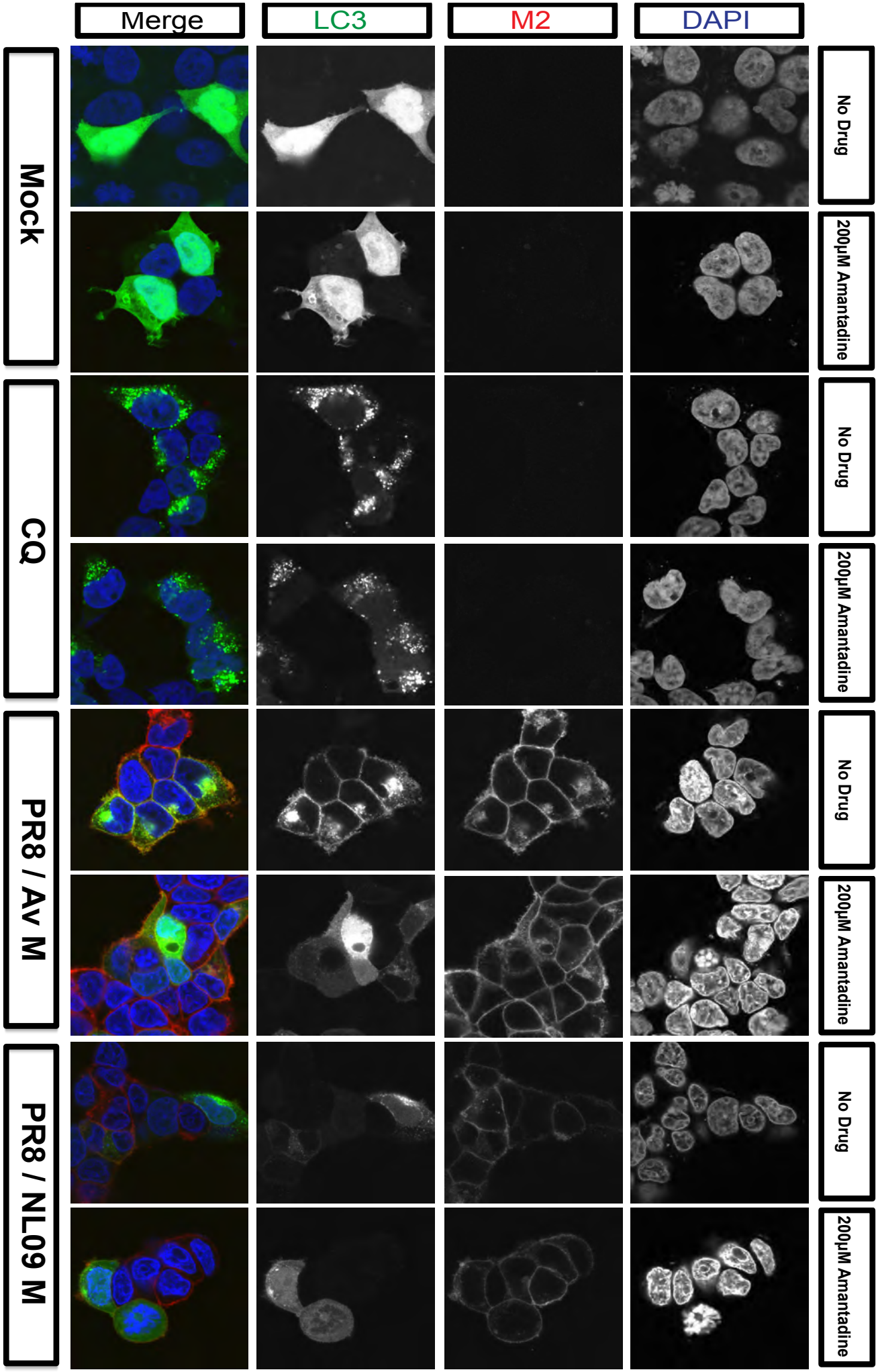
Merge
LC3
M2
DAPI
No Drug
200μM Amantadine
No Drug
200μM Amantadine
No Drug
200μM Amantadine
No Drug
200μM Amantadine
Mock
CQ
PR8 / Av M
PR8 / NL09 M

Figure 11

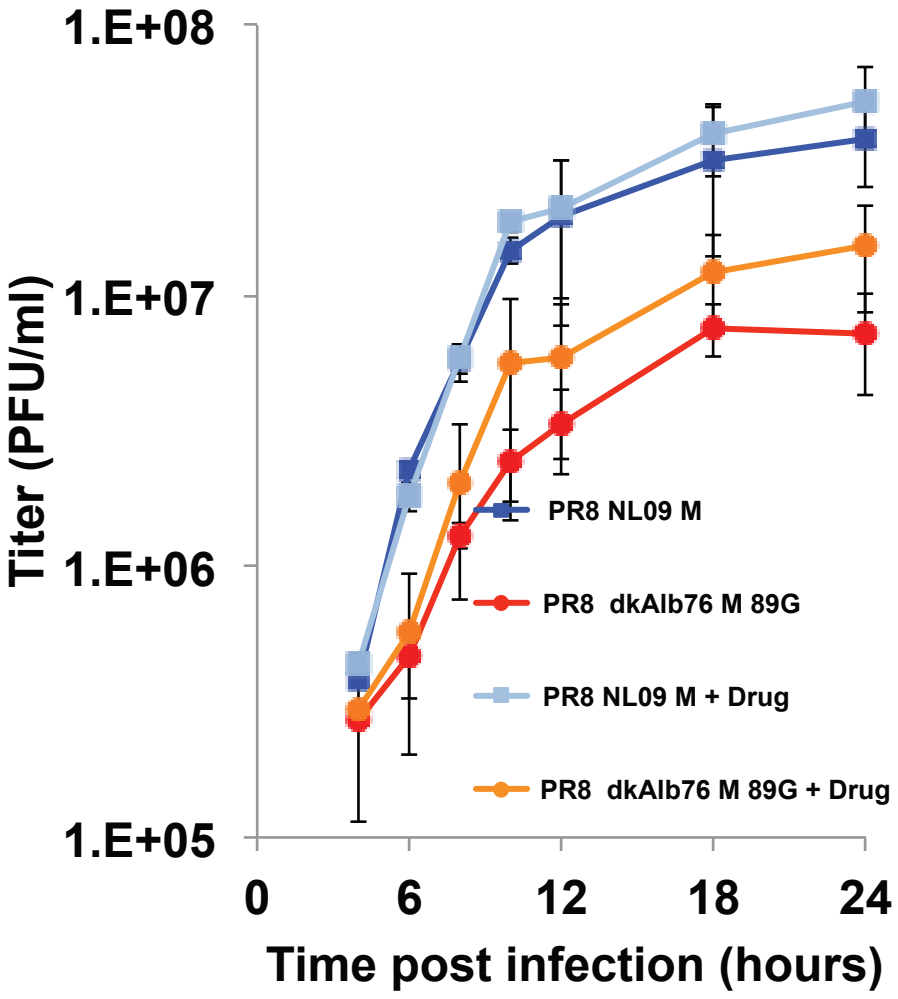
1.E+08
1.E+07
1.E+06
1.E+05
Titer (PFU/ml)
0
6
12
18
24
Time post infection (hours)
PR8 NL09 M
PR8 dkAlb76 M 89G
PR8 NL09 M + Drug
PR8 dkAlb76 M 89G + Drug

Figure 12

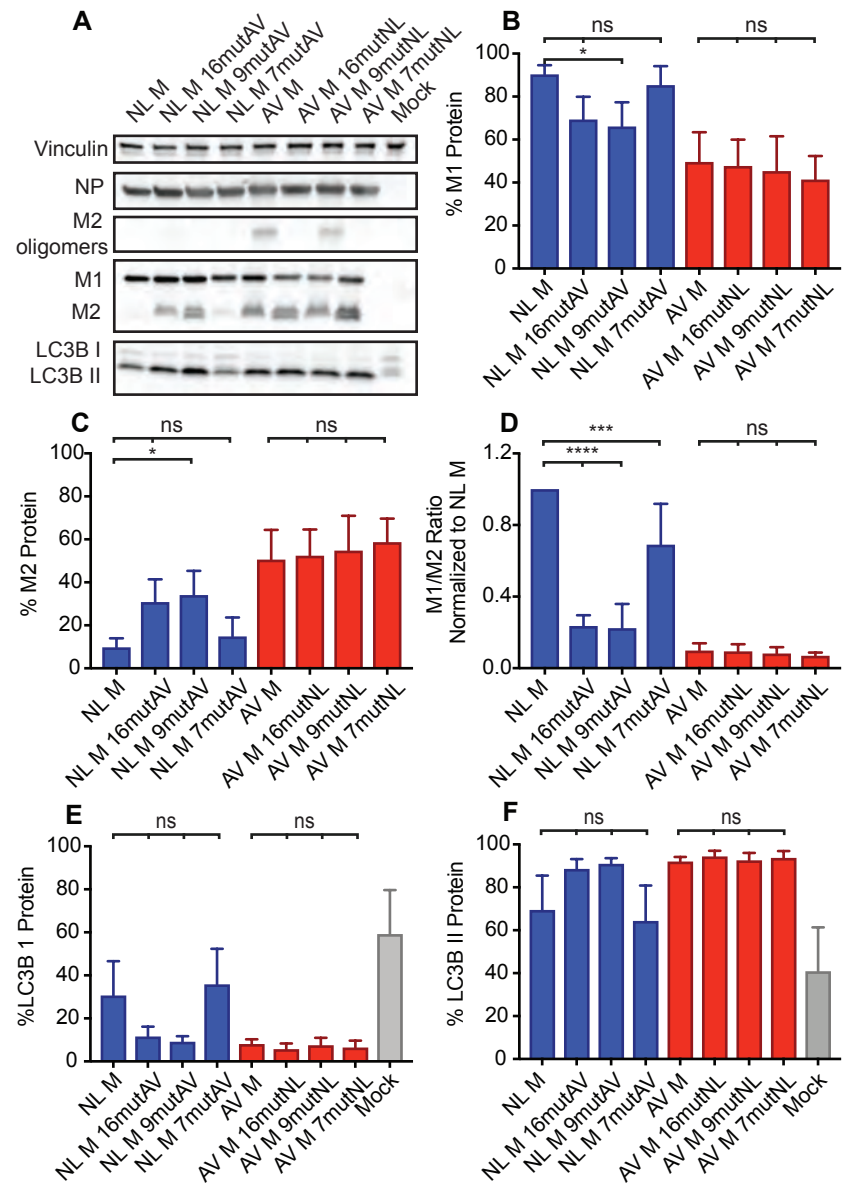
A
NL M
NL M 16mutAV
NL M 9mutAV
NL M 7mutAV
AV M
AV M 16mutNL
AV M 9mutNL
AV M 7mutNL
Mock
Vinculin
NP
M2 oligomers
M1
M2
LC3B I
LC3B II
B
% M1 Protein
ns
*
C
% M2 Protein
D
M1/M2 Ratio Normalized to NL M
***
****
E
%LC3B 1 Protein
F
% LC3B II Protein

Figure 13

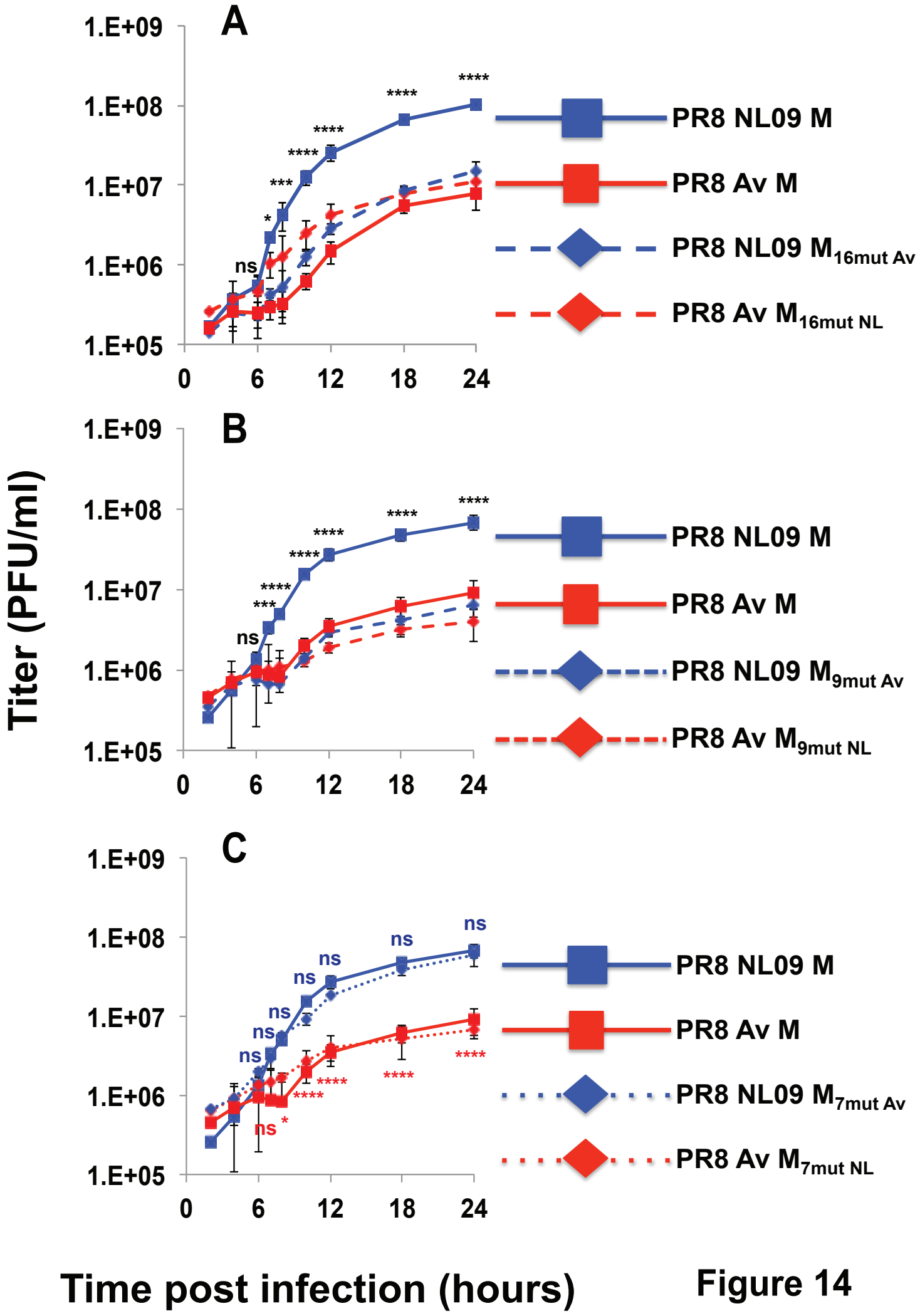
A
B
C
Titer (PFU/ml)
1.E+09
1.E+08
1.E+07
1.E+06
1.E+05
0
6
12
18
24
ns
*
***
****
PR8 NL09 M
PR8 Av M
PR8 NL09 M16mut Av
PR8 Av M16mut NL
PR8 NL09 M9mut Av
PR8 Av M9mut NL
PR8 NL09 M7mut Av
PR8 Av M7mut NL
Time post infection (hours)

Figure 14

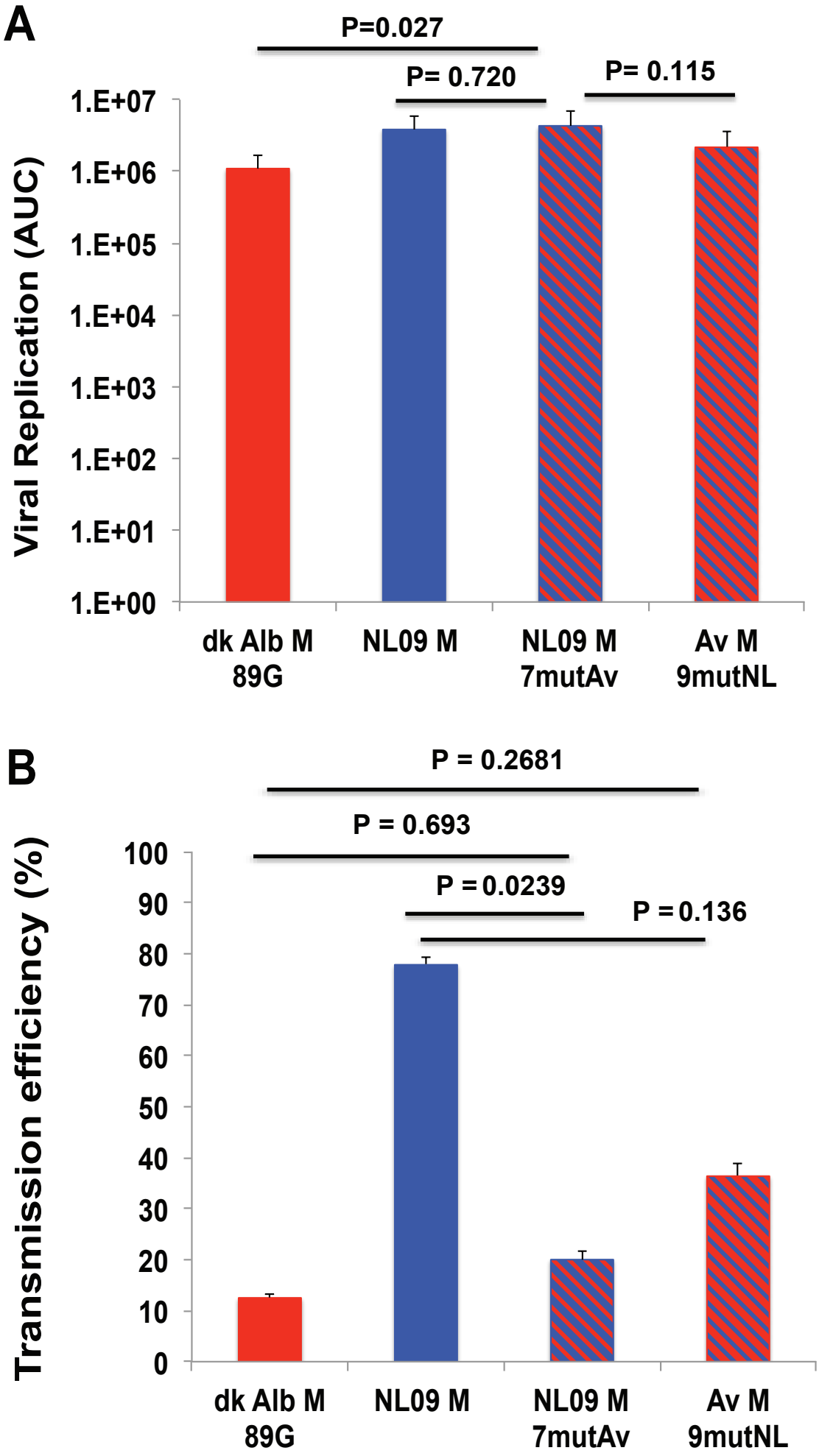
A
P=0.027
P= 0.720
P= 0.115
Viral Replication (AUC)
1.E+07
1.E+06
1.E+05
1.E+04
1.E+03
1.E+02
1.E+01
1.E+00
dk Alb M 89G
NL09 M
NL09 M 7mutAv
Av M 9mutNL
B
P = 0.2681
P = 0.693
P = 0.0239
P = 0.136
Transmission efficiency (%)
100
90
80
70
60
50
40
30
20
10
0
dk Alb M 89G
NL09 M
NL09 M 7mutAv
Av M 9mutNL

Figure 15